博士論文

Dendrobium officinale extract fermented with a plant-derived lactic acid bacterium enhances the protection effect on UV-mediated skin photoaging

（皮膚光老化予防効果を指標とした植物乳酸菌の生薬発酵技術による新たな保健機能性の探索研究）

2024 年 3 月

広島大学大学院　　医学系科学研究科

2020 年度入学

D205995　費維成

Catalogue

Abstract

Plant-derived raw materials contain the bioactive compounds having potential anti-aging properties. Fermentation of these materials enhances nutrient availability and efficacy, sparking increased interest in herbal extracts and probiotics. While *Lactobacillus plantarum* has been isolated from various plants and fruits, its isolation from *Dendrobium officinale* is novel. In this study, 23 *L. plantarum* strains were isolated as potential candidates from *D. officinale* as its symbiotic bacteria. Five strains with a high degree of nutrient enrichment were selected for further study. The fermentation kinetics of *D. officinale* by these *L. plantarum* strains were investigated, employing free radical scavenging assay using 1,1-diphenyl-2-picrylhydrazyl (DPPH) and 2,2'-azino-bis-3-ethylbenzthiazoline-6-sulphonic acid (ABTS), ferric reducing antioxidant power (FRAP) assay, and oxygen radical absorbance capacity (ORAC) assay. *L. plantarum* GT-17F was identified as having superior antioxidant properties.

Metabolomics analysis of *D. officinale* fermented with *L. plantarum* GT-17F was performed, establishing principal component analysis (PCA) and volcano map multidimensional statistical models. Compared to the unfermented control group, 13 up-regulated and 2 down-regulated metabolites were identified in the fermented group. Levels of certain amino acids, lipids, and ketones in the differential metabolites were significantly increased, while some other amino acids decreased. Principal metabolites identified are 16-ketoestradiol, lucidenic acid K, tolfenamic acid, anisodamine, 5-L-glutamyl-L-alanine, and madlongiside C. *In vitro* studies revealed that the defense against UV-induced photoaging the fermented *D. officinale* extract is bolstered. This includes heightened free radical scavenging, attenuation of collagen type I and III degradation, restoration of epidermal barrier functions, and diminished impairment to barrier-specific proteins, filaggrin (FLG) and loricrin (LOR). Further study will be necessary to decode the exact biochemical transformations in *D. officinale* during fermentation with *L. plantarum* GT-17F.

Foreword

With rising consumer awareness, there is an increasing demand for cosmetics that are green, natural, safe, and health-promoting. Plant raw materials with guaranteed safety for manufacturing cosmetics are attracting attention as having high marketability [1]. Plant resources are rich in active ingredients, offering unique benefits in anti-inflammatory, antioxidant, moisturizing, and skin-whitening applications[2]. However, the concentration of these active compounds in natural plants is often low, and their complex structures may sometimes exhibit toxic side effects, posing challenges in cosmetic raw material development[3, 4]. Fermentation technology related to increase of microbial activity and the controlled processing, enables the large-scale production of fermented products[5]. It can increase the concentration of active ingredients in plants, enhance efficacy, and reduce toxicity, thereby improving the safety and effectiveness of plant-based cosmetic and food ingredients[6].

Many commercial *Lactobacillus* species are derived from animal sources, predominantly fermented dairy products and the human gut[7]. Most commercial *Lactobacillus* species on the market are isolated from animal sources represented by fermented dairy products and human intestines[8, 9], which are suitable for high-protein fermentation environment and have higher metabolic efficiency for lactose[10]. In contrast, the plant-derived *Lactobacillus* strains, which are adapted to fructose and glucose utilization, are more suitable for fruit and vegetable fermentation[11]. Furthermore, the physical and chemical characteristics of fresh fruits, vegetables, and plants, such as intense UV radiation, elevated temperatures, and the presence of nutrients and antimicrobial compounds, closely resemble the human skin environment[12]. Adapted to plant-based environments, plant-derived *Lactobacillus* strains not only exhibit enhanced fermentation efficiency[13], but may also have skin tolerance rates comparable to or surpassing those of animal-derived *Lactobacillus* strains[11]. Thus, exploring and utilizing plant-derived *Lactobacillus* strains can diversify strain sources for fermented foods and cosmetics and provide valuable

resources for skin and intestinal health, especially relevant to East Asian populations[14–17].

Current research on *Dendrobium officinale* primarily focuses on its polysaccharides, noted for their anti-inflammatory, antioxidant, and anti-aging properties[18]. Additionally, fermentation can break down the large molecular substances in *D. officinale* into smaller molecules, enhancing biological activity, improving human absorption, and potentially reducing production costs[19]. However, research into the active components and functions generated by the fermentation of *D. officinale* with *Lactobacillus plantarum*, particularly regarding anti-aging effects, remains limited. This study investigates the fermentation of *D. officinale* using *L. plantarum*, assessing the differences of anti-aging activity before and after fermentation through *in vitro* and *in vivo* experiments, to evaluate its potential application in skin anti-photodamage and anti-aging cosmetics.

Chapter 1

Isolation and screening of *Lactobacillus plantarum*

1.1 Introduction

Currently, a significant number of *Lactobacillus* strains are isolated from fermented food products like pickles and sauces. However, plant-derived *Lactobacillus* strains, especially those in natural environments, are less extensively explored and developed[20]. Many natural plants, including those that decay, harbor a proportion of *L. plantarum*. These symbiotic *L. plantarum* strains, surviving alongside new plant growth in natural environments, endure harsh conditions such as extreme temperature fluctuations, strong ultraviolet radiation, and high humidity[21, 22]. This adaptability potentially endows them with higher fermentation efficiency and the ability to convert certain challenging substances or antibacterial compounds. Therefore, a wide range of *L. plantarum* strains can be extracted and examined from the natural habitat of *D. officinale* in highly productive regions, making them suitable microorganisms for fermenting *D. officinale*. This chapter describes the use of traditional culture methods and molecular biology techniques for the isolation, purification, and identification of *Lactobacillus* strains from *D. officinale* samples collected in Longling, Yunnan, China. The aim is to provide valuable strain resources for the fermentation of *D. officinale*.

1.2 Materials

1.2.1 Sample information

Sampling Site: Long ling County, Yunnan Province, China

Sampling Time: 2020.6.13-15

Longitude and Latitude: 98.68, 24.49

Temperature and Humidity: 25℃±5℃, 60%±20%

Table 1. *Dendrobium officinale* sample numbers.

Root	Stem	leaf	Flower	Soil
50	50	30	20	50

1.2.2 Reagents

Table 2. Main reagents used in the experiment.

Experiment reagent	Manufacturer
MRS medium $CaCO_3$ NaCl Tris EDTA-2Na	Sinopharm Chemical Reagents Co., Ltd
6×Loadding buffer Cetyltrimethylammonium bromide (CTAB) 10× PCR buffer Agarose Primer 27F 5’-AGAGTTTGATCCTGGCTCAG-3’ Primer 1495R 5’-CTACGGCTACCTTGTTACGA-3’	Sangon Biotech (Shanghai) Co.,Ltd

1.2.3 Instrument

Table 3. Main instrument used in the experiment

Instrument	Manufacturer
Vortex-2 Vortex mixer	Shanghai Huxian Industrial Co., Ltd
LRH-70 biochemical incubator	Shanghai Yiheng Technology Co., Ltd
YXQ-sII pressure steam sterilization pot	Boxun Industrial Co., Ltd
ABI Veriti 96-well gradient PCR instrument	Applied Biosystems, Inc
UVP CDS-8000 gel Imaging Analysis system	Beijing Liuyi Instrument Plant
DYY-12 electrophoresis apparatus	
SW-CJ-2D ultra clean table	Suzhou Purification Equipment Co., Ltd
CR21N high speed refrigerated centrifuge	Hitachi, LTD
HH-3 thermostatic water bath	Jintan Instrument Factory

1.3 Methods

1.3.1 Isolation and purification of *Lactobacillus*

The samples of *D. officinale* were diluted from 10^{-1} to 10^{-5} gradient by the double dilution method, and the dilutions of 10^{-2}, 10^{-3} and 10^{-4} gradient were coated on MRS Solid plates supplemented with 1.0% (w/v) calcium carbonate, and the samples were incubated in inversion for 48 h at 35°C. Single colonies with transparent circles with different shapes, sizes and colors were selected and crossed three times in a row, and then transferred to 5 mL MRS liquid test tube for culture at 35℃ for 24 h. Finally, the bacteria of Gram staining positive strains were collected, 1 mL of 30% (v/v) glycerol was added, and frozen in the refrigerator at -80℃ for later use.

1.3.2 Identification of *Lactobacillus*

Using cetyl trimethyl ammonium bromide (Hexadecyltrimethylammonium Bromide, CTAB) method of DNA extraction and separation of *Lactobacillus* strains. PCR

reaction system is prepared (2.5 μL dNTP mix, 2.5 μL 10×PCR buffer (Mg^{2+}), 0.5 μL primer, 0.2 μL rTaq, 0.2 μL DNA, add H_2O to 25 μL), and PCR reaction condition is designed (1min, 94℃; 45 sec, 94℃, 30 cycles; 45 sec, 55℃; 90 sec, 72℃; 10 min, 72℃; ∞, 72℃). After the amplification, 2.5 μL PCR samples underwent agarose gel electrophoresis, and the recovered products were chosen based on the presence of distinct bands and absence of any noticeable tailing. Afterwards, the recovered products were connected to pMD18-T vector and transformed into capable *Escherichia coli* top10 (Table 5). The clones that yielded positive identification results were chosen and dispatched to Tsingke Biotechnology Co., Ltd for sequencing, and the sequencing results returned by splicing were submitted to the National Center for Biotechnology Information, USA. NCBI) to determine whether it was *L. plantarum*.

1.4 Results

1.4.1 Microbial colony appearance and colony morphology

The preliminary screening of *Lactobacillus* was carried out by the colony morphology grown on MRS+$CaCO_3$ solid medium. Under aerobic conditions, most of the strains formed milky white or translucent, indicating rough colonies with irregular edges. At the same time, because the acid metabolites produced by *Lactobacillus* would react with $CaCO_3$, a clear transparent circle appeared on the plate. This is shown in Figure 1. By observing the morphology of the colonies, we selected a total of 457 suspected *Lactobacillus* strains from the specimens.

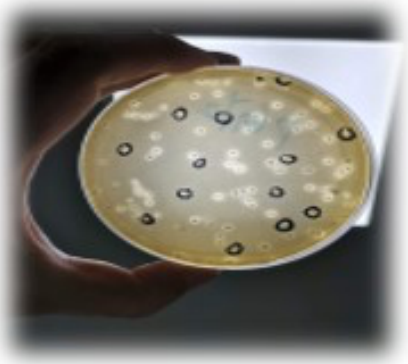

Figure 1. Transparent circle of *Lactobacillus*.

1.4.2 Sequencing results of *Lactobacillus* 16S rDNA PCR products

After comparing the sequencing outcomes of 16S rDNA PCR samples from the chosen 457 suspected *Lactobacillus* on NCBI BLAST, it was found that 107 *Lactobacillus* exhibited significant similarity to *L. plantarum* 23 strains with high homology with *L. plantarum* were obtained by screening the duplicate results (Table 4).

Table 4. Results of the BLAST.

Strain code	Approximate strain	similarity
NHF1	*Lactobacillus plantarum* strain 7232	100%
D13	*Lactobacillus plantarum* SN13T	99.70%
9-6	*Lactobacillus plantarum* strain 1940	100.00%
C1	*Lactobacillus plantarum* strain 27320	99.38%
2-6	*Lactobacillus plantarum* strain 3334	100.00%
74D	*Lactobacillus plantarum* strain 3335	100%
NHD2	*Lactobacillus plantarum* strain 3365	100%
NHF7	*Lactobacillus plantarum* strain 3356	100%
ZA6	*Lactobacillus plantarum* strain 3757	100%
33B	*Lactobacillus plantarum* strain 4310	100.00%
A14	*Lactobacillus plantarum* strain 7232	100.00%
GT17F	*Lactobacillus plantarum* strain 7232	99.90%
2-3	*Lactobacillus plantarum* strain 84L	100%
77C	*Lactobacillus plantarum* strain 8594	100%
A25	*Lactobacillus plantarum* strain BIOUAL002	99.60%
A24	*Lactobacillus plantarum* strain FB003	94.50%
77B	*Lactobacillus plantarum* strain KCC48	100%
ZB1	*Lactobacillus plantarum* strain SDMCC050424	100%
78A	*Lactobacillus plantarum* strain LLA360	99.90%
68B	*Lactobacillus plantarum* strain PT0015	99.90%
17D	*Lactobacillus plantarum* strain SDMCC050424	100%
L5-13	*Lactobacillus plantarum* strain WS17	99.90%
77A	*Lactobacillus plantarum* strain Y	100%

1.5 Discussion

While the isolation of *L. plantarum* from various plants and fruits is well-documented, its isolation specifically from *D. officinale* has not been previously reported. The isolation of *Lactobacillus* lacks a strictly selective medium. The MRS Medium used in this study serves as a semi-selective medium for *Lactobacillus*, which also supports the growth of various enterococci, enterobacteria, streptococci, and staphylococci. However, upon comparing the colony morphology under aerobic conditions, it was observed that colonies exhibiting opalescent or translucent appearances, with rough, flat surfaces and irregular edges, were predominantly identified as *Lactobacillus*. Although some *Lactobacillus* colonies can also appear milky white, round, smooth, and neatly edged under aerobic conditions, they closely resemble *Enterococcus* and *Streptococcus* colonies, making differentiation challenging. The selection specificity for *Lactobacillus* was enhanced by choosing milky white or translucent colonies, which have rough, flat surfaces and irregular edges, under aerobic conditions. Ultimately, these potential strains were identified using 16S rDNA PCR analysis, leading to the selection of 23 *L. plantarum* strains as our candidates.

Chapter2

Dendrobium officinale fermentation technology and selection of fermentation *Lactobacillus plantarum*

2.1 Introduction

The rising interest in aesthetics and well-being has amplified the focus on fermented products derived from non-dairy sources, such as herbs and produce. This shift underscores the importance of assessing the effectiveness and nutritional value of these products. *D. officinale* is known to contain beneficial components like polysaccharides, minerals, amino acids, alkaloids, and polyphenols. Traditionally, fresh *D. officinale* is processed using heat to create 'iron sheet maple bucket,' a form suitable for storage and transport. However, heat processing as a preservation method for these medicinal materials can result in nutrient loss in *D. officinale*, altering its taste and color, and potentially reducing its efficacy.

D. officinale juice, retaining full efficacy and nutritional value, offers a smooth taste and tangy fragrance, making it increasingly popular. Yet, the juice's composition can vary with different processing methods. High temperature blanching, a common pretreatment in fruit and vegetable processing, helps protect color and deactivate enzymes, while pasteurization can eliminate bacteria at lower temperatures, maintaining the original flavor and reducing nutrient loss.

L. plantarum, a commonly used *Lactobacillus* species in plant food fermentation, can enhance the nutritional content and shelf life of fermented products. The fermentation activity of *Lactobacillus* is closely linked to the fermentation substrate, and selecting the appropriate strain is crucial. Analysis of previously screened *L. plantarum* revealed that five strains, GT-17F, NHF7, L5-13, ZB1, and 77A, were predominant among the 107 strains. These strains displayed strong acid-producing

capabilities, indicated by their large transparent zones. Based on the fermentation conditions of these five strains, fermentation kinetic parameters were determined. The antioxidant capacities of these *L. plantarum* strains were evaluated using methods such as free radical scavenging assay using 1,1-diphenyl-2-picrylhydrazyl (DPPH) and 2,2'-azino-bis-3-ethylbenzthiazoline-6-sulphonic acid (ABTS), ferric reducing antioxidant power (FRAP) assay, and oxygen radical absorbance capacity (ORAC) assay. Therefore, this section primarily focuses on screening the target *L. plantarum* strains from these five candidates for subsequent research.

2.2 Materials

2.2.1 Reagents

Table 5. Main reagents used in the experiment.

Experiment reagent	Manufacturer
D. officinale	Dendrobium Germplasm Resource Center (Long ling, Yunnan, China)
2,2-diphenyl-1-picrylhydrazyl (DPPH) assay kit, ferric reducing antioxidant power (FRAP) assay kit 2-2'-azino-bis (3-ethylbenzthiazoline-6-sulfonic acid) (ABTS) assay kit	Beyotime Biotech. Inc.
CheKine™ Oxygen Radical Antioxidant Capacity (ORAC) Fluorometric Assay Kit	Abbkine Scientific Co., Ltd

2.2.2 Instrument

Table 6. Main instrument used in the experiment.

Instrument	Manufacturer
Vortex-2 Vortex mixer	Shanghai Huxian Industrial Co., Ltd
PHSJ-5 pH meter	Shanghai Precision Scientific Instrument Co., Ltd
YXQ-sII pressure steam sterilization pot	Boxun Industrial Co., Ltd
Infinite M200 Pro microplate reader	Tecan (Shanghai) Trading Co., Ltd
CR21N high speed refrigerated centrifuge	Hitachi, LTD
HH-3 thermostatic water bath	Jintan Instrument Factory

2.3 Methods

2.3.1 Preparation of *Dendrobium officinale* juice

Fresh *D. officinale* → Wash → cut (2-3cm) → beat → filter →*D. officinale* juice

2.3.2 Inoculation and fermentation

The activated L5-13, NHF7, ZB1, GT-17F, 77A *L. plantarum* solution was collected by centrifugation, and the bacteria were mixed with the same amount of normal saline. The bacteria were inoculated into *D. officinale* juice at 1% (v/v) ratio, and fermented and cultured in a shaker at 35±2℃ for 48 h. Samples were taken at 0 h, 12 h, 24 h, 36 h, and 48 h, and subsequently placed in a refrigerator set at a temperature of 4 °C. At the same time, according to the same conditions, a *D. officinale* juice without *L. plantarum* was prepared. After 48 h, it was sterilized at 121℃ for 20 minutes. The fermentation broth of *L. plantarum* and the unfermented *D. officinale* juice were centrifuged by centrifuge, and the supernatant was taken, passed through a 0.22 μm filter membrane, and freeze-dried. *L. plantarum* fermentations FDO-L5-13, FDO-NHF7, FDO-ZB1, FDO-GT-17F, FDO-77A and unfermented extract *D. officinale* (DO)

were obtained.

2.3.3 Calculation of overall acidity level

A volumetric flask with a capacity of 250 mL was used to draw 25.0 mL of the fermentation broth using a pipette. The volume was then adjusted by adding carbon dioxide-free water. For scaling purposes, vigorously shake the solution, then filter it using a rapid filter paper to collect the resulting filtrate, which will be utilized for determination. To the test solution, 50 mL of the solution was added with 2~4 drops (10 g/L) of phenolphthalein indicator solution. Then, titration was carried out using a 0.1 mol/L standard solution of sodium hydroxide until a faint red color persisted for 30 seconds without fading. For the blank experiment, an equal volume of carbon dioxide-free water was substituted for the test solution, and the amount of standard sodium hydroxide solution consumed was noted.

Formula of calculation:

$$X = \frac{[c\times (V1 - V2)]\times k\times F}{m}\times 1000$$

X - The total acidity level in the sample is measured in grams per liter (g/L);

c - Concentration of the standard solution of sodium hydroxide in moles per liter;

V 1 - Volume (mL) of sodium hydroxide standard solution consumed when titrating the test solution;

V 2- represents the amount of sodium hydroxide standard solution used in the blank test, measured in milliliters, while k is the conversion coefficient for acid;

F - dilution of the test solution;

m- mass of test solution (mL);

The outcomes are presented as the average of two separate measurements acquired under conditions of repeatability, and the outcomes are kept to two decimal points.

2.3.4 Measurement of acidity level and assessment of live bacterial population

FDO-L5-13, FDO-NHF7, FDO-ZB1, FDO-GT-17F, and FDO-77A were tested at 0 h, 12 h, 24 h, 36 h, and 48 h using a pH meter. At the same time, samples were taken

at these time points, and the number of viable bacteria was calculated by dilution coating plate.

2.3.5 DPPH radical scavenging experiment

(1) Configure DPPH solution

6.0mg DPPH was accurately weighed using an analytical balance, added to a 100mL beaker, and then dissolved in an ultrasonic cleaning instrument by adding 40mL 95% ethanol. The mixture was mixed every 5min until completely dissolved. The DPPH solution was moved to a 50mL volumetric flask of brown color and titrated with 95% ethanol to achieve a concentration of 0.12mg/mL DPPH solution. Subsequently, this solution was transferred to a 100mL reagent flask of brown color and kept in the dark at 4 °C.

(2) The positive control was prepared

To verify the experimental system, Vitamin E was dissolved in ethanol with a concentration of 95% and then diluted into a series of concentration gradients, including 0.08, 0.04, 0.02, and 0.01 mg/mL.

(3) Sample dilution

Distilled water gradients were used to dilute the samples at concentrations of 10 mg/mL, 5mg/mL, 1mg/mL, 0.5 mg/mL, 0.1 mg/mL, 0.05 mg/mL, and 0.01 mg/mL.

(4) The sample was added according to the table below, and the reaction was shielded from light for 15min. The absorbance was detected at 517nm using a microplate reader.

Table 7. DPPH clearance test group.

Reagent	**Group**			
	T	**T_0**	**C**	**C_0**
Sample	50μL	50μL	/	/
VE	100μL	100μL	150μL	150μL
DPPH	50μL	/	50μL	/
95% ethanol	/	50μL	/	50μL
Number parallels	3	3	3	3

（5）computing method

DPPH radical scavenging was calculated and calculated according to the formula.

$$X=\left(1-\frac{T-T_0}{C-C_0}\right)\times 100\%$$

X—DPPH clearance of samples, %.

T—The absorbance measurement of the sample tube, specifically the absorbance value of the solution following the interaction between the sample and DPPH.

T_0—T0 refers to the initial absorbance value of the sample.

C—The average of three times of DPPH tube absorbance values, that is absorbance value of DPPH solution without adding samples.

C_0—Solvent background absorption value.

2.3.6 FRAP iron ion reduction experiment

According to the detection limit of the kit and the results of the preliminary experiment, the sample to be tested was diluted with distilled water at 10 mg/mL, 5 mg/mL and 1 mg/mL, and three groups of parallel experiments were set up. FRAP kit was used for detection, and the concentration falling within the standard curve was selected for calculation. Trolox dissolved in 80% methanol was used as a standard sample as a standard curve to calculate the antioxidant capacity of Trolox equivalent.

2.3.7 Evaluation of the capacity to scavenge ABTS free radicals

According to the detection limit of the kit and the results of the preliminary experiment, the sample to be tested was diluted in distilled water to 10 mg/mL, 5 mg/mL and 1 mg/mL, and three groups of parallel experiments were set up. ABTS kit was used for detection, and the concentration falling within the standard curve was selected for calculation. Trolox dissolved in 80% (v/v) methanol was used as a standard sample as a standard curve to calculate the antioxidant capacity of Trolox equivalent.

2.3.8 Measurement of the capacity to scavenge ABTS free radicals

The determination was conducted using the ORAC fluorescence detection kit,

following the kit's operation instructions. The 96-well plate was preheated at 37℃, and then 150 μL of fluorescein solution was added to the plate. Subsequently, 25 μL of Trolox standard and the sample under examination were added, followed by an incubation period of 10 minutes at 37℃. Afterward, 25 μL of working solution containing 2, 2' -azo bis (2-methylpropyl imidine) dihydrochloride was introduced, and the absorbance was determined at 520 nm. Trolox dissolved in 80% (v/v) methanol was used as a standard sample as a standard curve to calculate the antioxidant capacity of Trolox equivalent.

2.4 Results

2.4.1 Analysis of fermentation characteristics of *Dendrobium officinale* juice fermented by different *Lactobacillus plantarum*

The growth of various *L. plantarum* in *D. officinale* juice exhibited significant variations after 12 h of fermentation, as depicted in Figure 2. In the comparison of viable bacteria number, FDO-77A > FDO-ZB1 > FDO-GT-17F > FDO-NHF7 > FDO-L5-13. It indicated that *L. plantarum* 77A grew fastest in *D. officinale* juice. In the whole fermentation process, 12–24h belongs to the logarithmic phase of *L. plantarum* growth, during which the biomass of *L. plantarum* increases the fastest. At 36h, all *L. plantarum* basically reach the stable period, and there is little difference in the biomass of each strain. The biomass of *Lactobacillus* in each plant does not change after 48h of fermentation, and this time point can be set as the end point of fermentation.

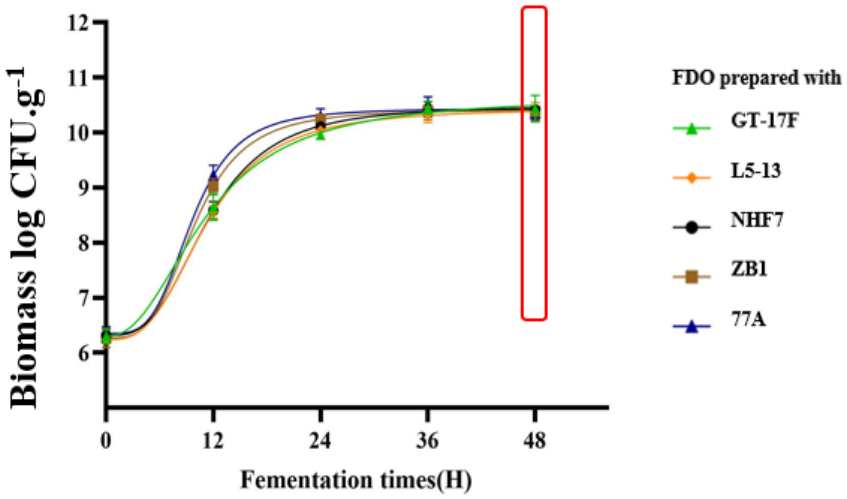

Figure 2. Biomass of different *Lactobacillus plantarum.*

The acid production capacity of various *L. plantarum* in *D. officinale* juice varied significantly after 48 h of fermentation, as depicted in Figure 3. In the comparison of acid production capacity, FDO-GT-17F > FDO-77A > FDO-ZB1 > FDO-NHF7 > FDO-L5-13. These results indicated that *L. plantarum* GT-17F had the strongest ability to produce acid during the fermentation process of *D. officinale* juice. During the whole fermentation process, the acid production of *L. plantarum* increased rapidly from 4–20h, which was proportional to the biomass of *L. plantarum*. After 48h of fermentation, the acid production of *L. plantarum* did not changes.

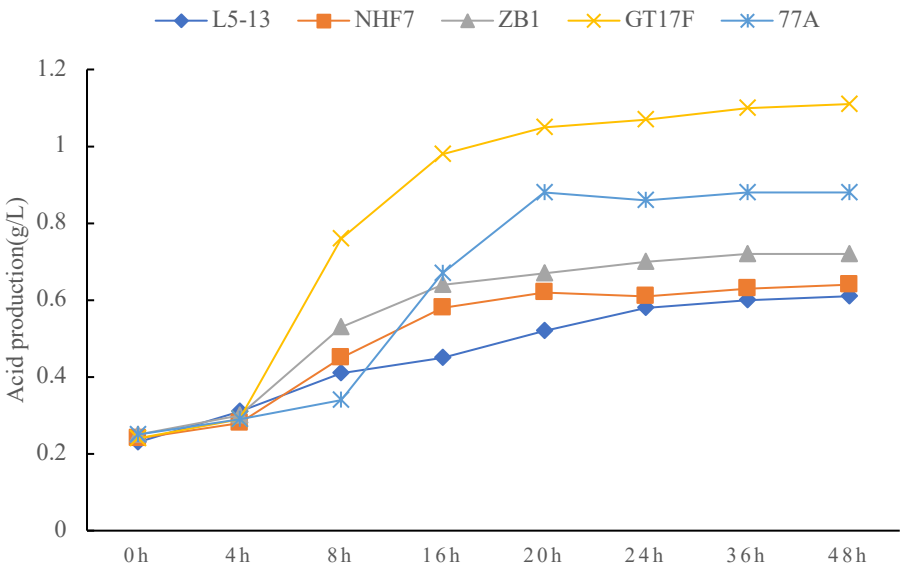

Figure 3. Results of acid production capacity of different *Lactobacillus plantarum.*

Figure 3 illustrates that various strains of *L. plantarum* exhibit distinct variations in *D. officinale* juice after 48 h of fermentation. Notably, *L. plantarum* GT-17F demonstrates the lowest pH in the fermentation broth, which directly correlates with bacterial biomass and acid production levels. After 48 h of fermentation, the pH of *L. plantarum* did not change.

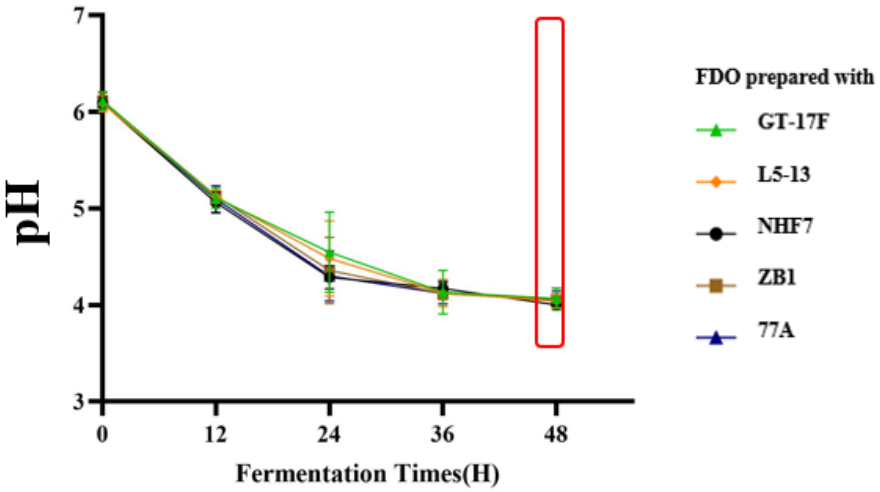

Figure 4. Results of pH of different *Lactobacillus plantarum.*

2.4.2 Changes of antioxidant capacity of different fermentation strains in *Dendrobium officinale* juice

To identify the most suitable *L. plantarum* strain for *D. officinale* fermentation, we initially screened the antioxidant activity of these strains, comparing them with unfermented *D. officinale*. DPPH assay results indicated that *L. plantarum* fermentation significantly enhanced the free radical scavenging capacity of *D. officinale*. Notably, *L. plantarum* GT-17F exhibited the lowest IC_{50} value for radical scavenging at 4.52 mg/mL, indicating superior antioxidant efficacy among the tested strains. Detailed results are presented in Table 8.

Table 8. DPPH scavenging experiment results.

Sample	DO	FDO GT-17F	FDO L5-13	FDO NHF7	FDO ZB1	FDO 77A
0.01 mg/ml	0.8±1.4	0.9±0.8	0.9±0.7	0.8±0.7	0.9±0.7	1.1±0.8
0.05 mg/ml	1.5±1.7	3.1±1.3	3.1±3.2	3.0±1.3	3.1±1.4	3.0±2.4
0.1 mg/ml	1.3±2.4	3.9±2.2	6.0±2.7	3.8±1.4	4.0±1.5	6.8±3.2
0.5 mg/ml	4.6±2.3	16.6±4.3***	14.6±4.0***	12.6±3.5***	14.1±2.8***	11.0±3.1*
1 mg/ml	11.9±2.4	22.5±2.4***	23.0±2.1***	21.3±0.8***	21.1±1.1***	22.5±2.2***
5 mg/ml	36.7±3.5	52.2±2.4***	50.1±3.4***	47.7±2.8***	49.2±2.6***	48.2±3.5***
10 mg/ml	53.4±3.9	71.1±2.8***	70.0±0.4***	68.1±4.0***	66.7±3.6***	69.5±2.0***
IC50	8.70	4.52	4.92	5.37	5.15	5.28

Note: Compared with DO samples, *, $p < 0.05$; ***, $p < 0.001$

According to the iron ion reduction ability test of FRAP, the standard curve fitting formula of Trolox is $y = 0.2075x + 0.0273$ ($R^2 = 0.9935$). The TE values of fermented *D. officinale* fermented by different *L. plantarum* are shown in Figure 5. The figure clearly shows that the TE value of *L. plantarum* GT-17F is considerably greater than the TE value of unfermented *D. officinale* (DO). At the same time, compared with FDO-77A, FDO-ZB, FDO-NHF7 is also significant.

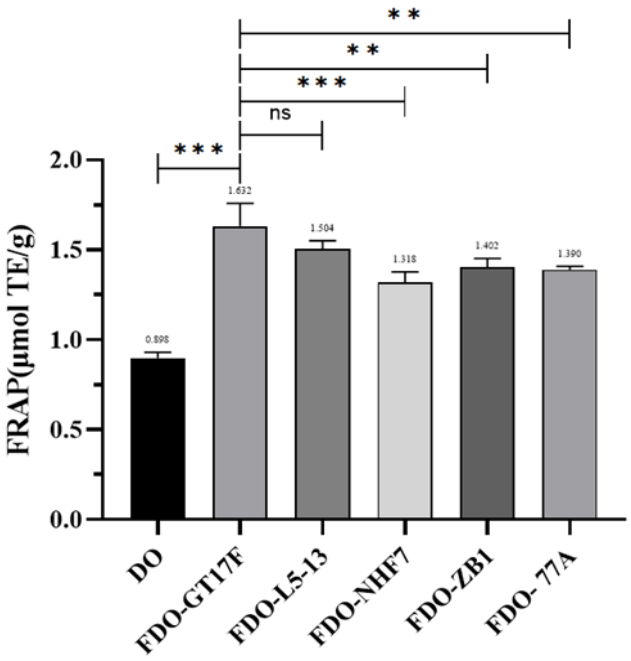

Figure 5. Antioxidant FRAP results of different *Lactobacillus plantarum* fermented *Dendrobium officinale*.

Note: The comparison of other experimental groups with the FDO-GT-17F group is denoted by an asterisk (*), indicating statistical significance at $p < 0.05$, ** at $p < 0.01$, and *** at $p < 0.001$.

According to the free radical scavenging test of ABTS, the standard curve fitting formula is $y = -11.812x + 18.138$ ($R^2 = 0.9988$). The TE values of fermented *D. officinale* fermented by different *L. plantarum* are shown in Figure 6. The figure clearly shows that the TE value of *L. plantarum* GT-17F is considerably greater than the TE value of unfermented *D. officinale* (DO). At the same time, compared with FDO-77A, FDO-ZB1, FDO-NHF7 is also significant.

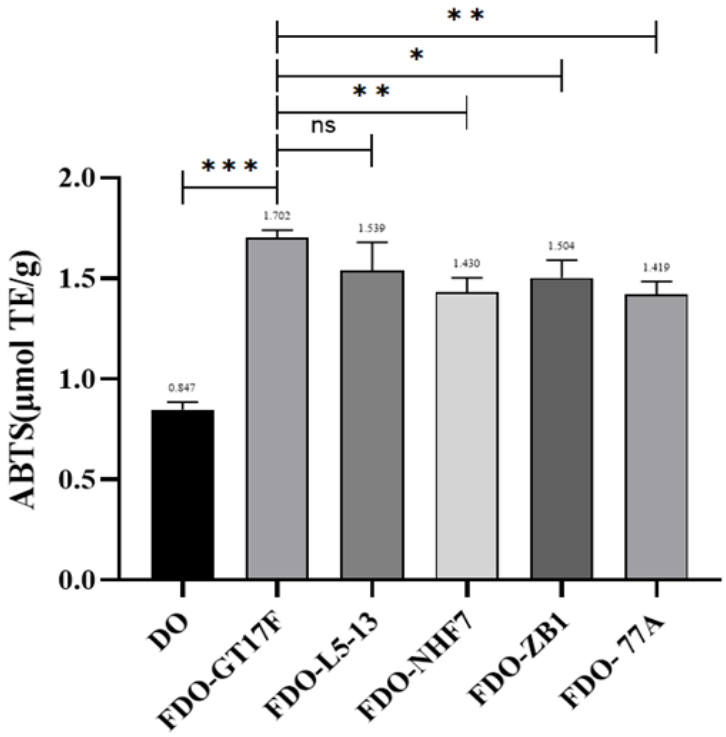

Figure 6. Antioxidant ABTS results of different *Lactobacillus plantarum* fermented *Dendrobium officinale.*

Note: The comparison of other experimental groups with the FDO-GT-17F group is denoted by an asterisk (*), indicating statistical significance at $p < 0.05$, ** at $p < 0.01$, and *** at $p < 0.001$.

According to the free radical scavenging test of ORAC, the standard curve fitting formula is $y = 0.1603x + 1.3976$ ($R^2 = 0.9962$). Figure 7 displays the TE values of *D. officinale* fermented by various strains of *L. plantarum*. The figure clearly shows that the TE value of *L. plantarum* GT-17F is considerably greater than the TE value of unfermented *D. officinale* (DO). At the same time, compared with FDO-77A, FDO-NHF7 is also significant.

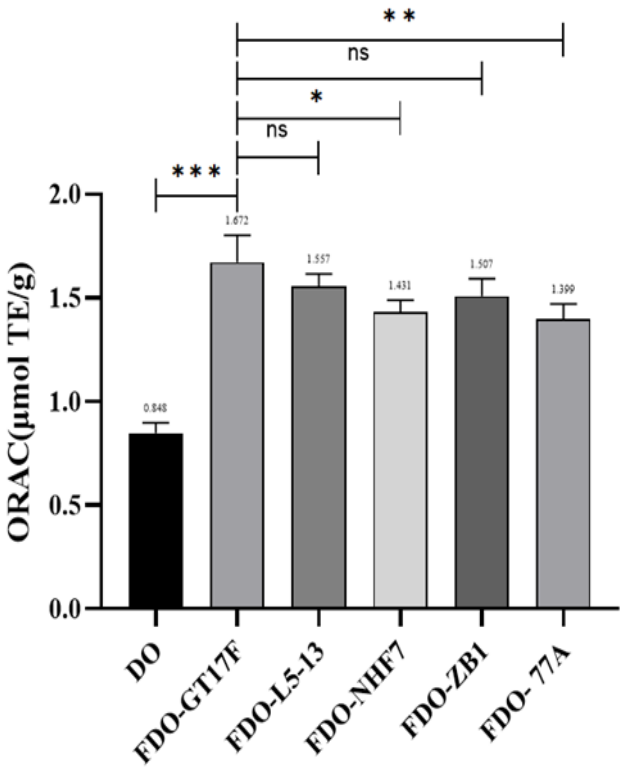

Figure 7. Antioxidant ORAC results of different *Lactobacillus plantarum* fermented *Dendrobium officinale.*

Note: The comparison of other experimental groups with the FDO-GT-17F group is denoted by an asterisk (*), indicating statistical significance at $p < 0.05$, ** at $p < 0.01$, and *** at $p < 0.001$.

2.5 Discussion

Optimal fermentation conditions promote the rapid proliferation of *Lactobacillus*, resulting in the outcompeting of non-native microorganisms or potential pathogens during the natural fermentation process, as evidenced by a bacterial count of 7.00 ~ 8.00 $\log_{10}$ CFU/mL after 24 h or 48 h of fermentation. The study found that the antibacterial properties of *Lactobacillus* obtained from plant sources were attributed to the synthesis of different compounds including organic acids, bacteriocins, carbon dioxide, hydrogen peroxide, diacetyl, ethanol, fatty acids, lactococcin, and biosurfactants[23–26]. The suppressive impact of natural compounds (primarily lactic acid and acetic acid) on other microorganisms is associated with the non-ionized structure of these compounds. These compounds permeate the cell membrane and detrimentally influence fundamental metabolic processes, such as lowering the

intracellular pH[27].Furthermore, certain *Lactobacillus* strains have the capability to generate bacteriocins, peptide or protein metabolites that exhibit strong inhibitory effects on numerous pathogens found in fermented[28].The mechanism of action can vary depending on the particular bacteriocin produced, which may involve disturbing the membrane potential, blocking DNA or RNA synthesis, disrupting the pH gradient, or releasing anions and/or cations from the cell[29]. Furthermore, the generation of carbon dioxide establishes a condition devoid of oxygen for microorganisms, thereby impeding the proliferation of potentially aerobic spoilage microorganisms[30].

The level of acidity is a crucial factor that significantly impacts the process of food fermentation, as it is intricately linked to both microbial activity and the alteration of phytochemicals' structure during fermentation. It helps to improve the stability of microorganisms against pathogenic and spoilers, and can change the flavor of products[31, 32]. During the whole fermentation process, the pH value of *D. officinale* juice showed a trend of rapid decline in the slow period and then relatively gentle (Figure 4). The primary reason for this is primarily due to the active metabolism of *Lactobacillus* during the initial phase of fermentation. This vigorous metabolism results in the dissociation of organic acids, causing the release of hydrogen ions and subsequently altering the solution's balance, leading to a decrease in the pH value[33].The increase of organic acids inhibited the growth and metabolism of *Lactobacillus* (which was also reflected in the slowdown of the number of viable bacteria in Figure 2 after entering the stable phase), resulting in a decrease in the efficiency of acid production[34] .

Lactobacillus can be influenced in two primary manners to enhance its anti-oxidative activity. The first method involves the liberation of uncomplicated phenolic compounds following acidification, while the second method entails the enzymatic breakdown of polymerized phenolic compounds during fermentation[35].In addition, *Lactobacillus* may themselves have antioxidant activity, which also explains the similar trend of DPPH, FRAP, ABTS, ORAC free radical scavenging capacity (Table 8, Figures 4, 6, and 7).Prior research has discovered that numerous *Lactobacillus* possess both enzymatic and non-enzymatic antioxidant mechanisms, effectively diminishing the

generation of cellular reactive oxygen species (ROS) to a non-threatening extent. Lee *et al.* found that *Lactobacillus casei* strain not only increased the content of polyphenols in the fermentation process, but also had its own antioxidant activity[36]. Microbes, when exposed to ROS, develop strategies to safeguard themselves against oxidative harm by producing enzymatic and non-enzymatic antioxidants, which have the capacity to eliminate ROS directly[37]. Kim *et al.* found that *Lactobacillus bulgaricus* 207 could inhibit lipid peroxidation by improving the scavenging activity and reducing ability of -OH free radicals[38]. Spyropoulos *et al.* reported strains of *Lactobacillus* fermentum and *Streptococcus thermophilus* strain showed significant antioxidant activity through superoxide dismutase (SOD) and reduced oxidative stress[39]. *Lactobacillus* have the capacity to release and enhance the synthesis of primary non-enzymatic antioxidants and fragrances associated with free radicals (such as glutathione or catalase). In their study, Veron *et al.* utilized *L. plantarum* S-811 for the fermentation of cactus pear juice[40]. They discovered that the antioxidant capability of the juice was enhanced as the levels of ferularic acid and caffeic acid derivatives rose. These compounds were found to function as reducing agents, scavengers of free radicals, and quenchers of singlet oxygen. Additionally, it stimulates the function or manifestation of antioxidant enzymes like glutathione and thioredoxin in cellular structures. Furthermore, *Lactobacillus* can additionally stimulate the synthesis of specific antioxidant biomolecules, like external polysaccharides, while demonstrating metal chelating capability. *In vitro* antioxidant capacity, the increase of free radical scavenging ability of *D. officinale* after fermentation was higher than that of unfermented *D. officinale*. Different strains had different improvement effects, and the best fermentation time was also different. After fermentation with *L. plantarum*, the antioxidant capacity of *D. officinale* juice increased in different degrees, which may be related to the increase and composition of polyphenolic substances. Some studies have shown that *Lactobacillus* fermentation may also improve its antioxidant capacity by converting large molecular polysaccharides into small molecular polysaccharides with stronger activity, and the extracellular polysaccharides produced by *Lactobacillus* also have a certain degree of antioxidant activity. In conclusion, *L. plantarum* GT-17F can improve the antioxidant

effect of *D. officinale* juice to varying degrees, and the effect is the best compared with other *L. plantarum*. The fermentation parameter of 35℃±2 for 48 h is more suitable, and it is used as the test strain for the composition change of *D. officinale* fermentation in the next section.

Chapter3

Analysis of components of *Dendrobium officinale* fermented by *Lactobacillus plantarum* GT-17F

3.1 Introduction

As a traditional processing method, fermentation can degrade anti-nutrient factors through the action of microorganisms, generate bioactive substances, and increase the bioavailability of active ingredients[41, 42]. *D. officinale* polysaccharide obtained by fermentation has good free radical scavenging ability and excellent metal chelating activity[43]. Research indicates that mixed bacterial fermentation can enhance the flavor and softness of the fermentation liquid, enrich it with active functional components, and improve the product's storage quality through the synergistic action of multiple strains[44, 45]. In this experiment, we dynamically analyzed the active components in *D. officinale* juices throughout the fermentation process, using fresh strips of *D. officinale* as raw materials and *L. plantarum* as the fermentation strain. The objective was to evaluate the impact of *L. plantarum* on the quality of *D. officinale* during fermentation and to explore the potential benefits of products derived from *L. plantarum* fermentation of *D. officinale*, aiming to provide feasibility analysis and technical insights for the development of high-efficacy *L. plantarum*-based products.

In recent years, metabolomics has developed rapidly. Qualitative and quantitative analyses of metabolites, collected from organism tissues or produced under specific environmental conditions, enable the identification and screening of differential metabolites. These are crucial for early disease diagnosis, pathogenesis research, clinical drug target discovery, and disease diagnostics[46]. Metabolomics, as proposed by Fiehn et al., and Metabonomics, as reported by Nicholson *et al.*, represent the two primary directions in contemporary metabolomics research[47]. Metabolomics is

predominantly applied in the study of microorganisms and plants, focusing on the exploration of differences in metabolite patterns among various cell types. Meanwhile, Metabonomics mainly focuses on the study of body fluids and tissues, emphasizing the comprehensive changes in the metabolite composition spectrum of the body under external toxicants, drugs, and environmental stimuli[48]. innovatively proposed the concept of pharmaceutical metabolomics, building on the foundation of metabolomics research, and applied its methods to drug efficacy evaluation, toxicity assessment, new drug development, and disease diagnosis[49].

Liquid chromatography-mass spectrometry (LC-MS) is currently the most widely employed technology in metabolomics research[50]. Compared with other conventional detection techniques, LC-MS has very good advantages in the precise identification and quantitative analysis of poor thermal stability and non-volatile metabolites. The use of ultra-performance liquid chromatography (UPLC) coupled with quadrupole-time of flight mass spectrometry (Q-TOF-MS) has become increasingly prevalent in metabolomics research[51, 52]. The primary objective of this research was to conduct a comprehensive analysis of the metabolites in *D. officinale* before and after fermentation by *L. plantarum* GT-17F. This analysis was conducted using UPLC coupled with liquid LC-MS technology. The aim was to systematically identify the primary metabolic compounds produced during the fermentation of *D. officinale* and to gain insights into the key metabolic pathways involved. This study established theoretical foundations for understanding the interaction mechanisms in the fermentation of *D. officinale* using *L. plantarum* GT-17F.

3.2 Materials

3.2.1 Instruments

Electronic balance, Soxhlet extractor, vacuum pump and associated filtering devices, rotary evaporator, ultrasonic cleaner, UV-Vis spectrophotometer, and water bath.

3.2.2 Reagents

95% ethanol, absolute ethanol, glucose, double distilled phenol, concentrated sulfuric acid, gallic acid, sodium carbonate, phosphomolybdotungstic acid test solution, rutin, sodium nitrite, sodium hydroxide, aluminum nitrate, oleanolic acid, vanillin, perchloric acid, phenolphthalide, sodium hydroxide, leucine, ninhydrin, potassium dihydrogen phosphate, sodium dihydrogen phosphate, ultra-pure water.

3.3 Methods

3.3.1 Metabolite Extraction

Conducting untargeted metabolomics analysis, we collaborated with Shanghai Majorbio Bio-Pharm Technology Co., Ltd. For each sample, 50 mg of solid material was introduced into a 2 mL centrifuge tube along with a 6 mm diameter grinding bead. Metabolites were extracted using 400 μL of an extraction solution (methanol: water = 4:1, v: v) containing 0.02 mg/mL of the internal standard (L-2-chlorophenylalanine). The samples underwent grinding with the Wonbio-96c frozen tissue grinder (Shanghai wanbo biotechnology co., LTD) for 6 minutes at -10°C and 50 Hz, followed by low-temperature ultrasonic extraction for 30 minutes at 5°C and 40 kHz. After leaving the samples at -20°C for 30 minutes, they were centrifuged for 15 minutes at 4°C and 13000 × g. The resulting supernatant was transferred to the injection vial for subsequent LC-MS/MS analysis.

3.3.2 Quality control sample

As part of the system conditioning and quality control process, a pooled quality control sample (QC) was prepared by mixing equal volumes of each individual sample. The QC samples were processed and analyzed using the same method as the analytical samples. This approach ensured representation of the entire sample set, with QC samples being injected at regular intervals (every 5 to 15 samples) to monitor the analytical system's stability.

3.3.3 (UPLC-MS/MS) analysis

In the LC-MS/MS analysis of the samples, the SCIEX UPLC-Triple TOF 5600 system, equipped with an ACQUITY HSS T3 column (100 mm × 2.1 mm i.d., 1.8 μm; Waters, USA), was employed. The experiment was conducted at Majorbio Bio-Pharm Technology Co. in Shanghai, China. The mobile phases, denoted as A and B, consisted of 0.1% formic acid in water: acetonitrile (19:1, v/v) for solvent A and 0.1% formic acid in acetonitrile: isopropanol: water (9.5:9.5:1, v/v) for solvent B. The elution program followed a specific gradient in positive ion mode: 0–3 min, 0% to 20% B; 3–4.5 min, 20% to 35% B; 4.5-5 min, 35% to 100% B; 5–6.3 min, hold at 100% B; 6.3–6.4 min, decrease to 0% B; 6.4–8 min, hold at 0% B. In negative ion mode, the separation gradient was: 0–1.5 min, 0% to 5% B; 1.5–2 min, 5% to 10% B; 2–4.5 min, 10% to 30% B; 4.5–5 min, 30% to 100% B; 5-6.3 min, hold at 100% B; 6.3–6.4 min, decrease to 0% B; 6.4–8 min, hold at 0% B. The flow rate was 0.40 mL/min and the column temperature was 40°C.

The UPLC system was integrated with a Triple TOF™ 5600+ quadrupole-time-of-flight mass spectrometer (Sciex, USA), featuring an electrospray ionization (ESI) source operational in both positive and negative ionization modes. Optimal operational conditions were established as follows: the source temperature was maintained at 50℃; curtain gas (CUR) was set to 30 psi; Ion Source Gas1 and Gas2 were both regulated at 50 psi. The ion-spray voltage floating (ISVF) parameters were adjusted to -4000V for negative mode and 5000V for positive mode. The declustering potential was fixed at 80V, while the collision energy (CE) was varied between 20 to 60 eV, using a rolling mode for MS/MS. The data were acquired in the Information Dependent Acquisition (IDA) mode, with detection spanning a mass range from 50 to 1000 m/z.

3.3.4 Data anlaysis

Data preprocessing for LC/MS raw results utilized Progenesis QI software (Waters Corporation, Milford, USA), generating a three-dimensional data matrix in CSV format. This matrix encompassed sample details, metabolite identities, and mass spectral intensities. Peaks corresponding to internal standards and recognized artefacts

(including noise, column bleed, and peaks from derivatization reagents) were excised from the matrix, followed by deduplication and pooling of peaks. Concurrently, metabolite identification was conducted through database queries, primarily utilizing resources such as the Human Metabolome Database (HMDB) (available at http://www.hmdb.ca/), Metlin (accessible at https://metlin.scripps.edu/), and the Majorbio Database.

Data analysis was conducted on the Majorbio Cloud platform (available at cloud.majorbio.com), a freely accessible online resource. Metabolic features that were detected in at least 80% of any sample group were considered for further analysis. Post-filtering, the lower limit of quantitation (LLOQ) was applied, where metabolites falling below this threshold had their minimum values imputed. Each metabolic feature underwent normalization by sum to mitigate errors stemming from sample preparation and instrumental instability. This process involved normalizing the response intensity of sample mass spectrum peaks using the sum normalization technique, leading to a normalized data matrix. Concurrently, variables in QC samples with a relative standard deviation (RSD) exceeding 30% were excluded. The data then underwent $\log_{10}$ transformation to generate the final data matrix for subsequent analyses.

Variance analysis was conducted on the preprocessed data matrix. The R package "ropls" (Version 1.6.2) was employed for principal component analysis (PCA) and orthogonal least partial squares discriminant analysis (OPLS-DA). A 7-cycle interactive validation process was applied to assess the model's stability. Metabolites meeting the criteria of VIP>1 and $p<0.05$ were identified as significantly different metabolites. VIP values were obtained from the OPLS-DA model, and p-values were generated using a student’s t-test.

Differential metabolites between the two groups were further analyzed by mapping them to their respective biochemical pathways. This pathway analysis was based on the KEGG database (http://www.genome.jp/kegg/). The metabolites were categorized based on the pathways they were associated with and their functional roles. Enrichment analysis was employed to determine whether a group of metabolites appeared in a specific functional node. This approach involved expanding the

annotation analysis from single metabolites to groups of metabolites. Python packages "SciPy.Stats" (https://docs.scipy.org/doc/scipy/) were utilized to perform enrichment analysis, aiming to identify the most relevant biological pathways for the experimental treatments.

3.3.5 Determination of compound content

In order to analyze the changes of material composition after fermentation of *D. officinale*, we refer to the determination method of tannin content in Pharmacopeia and established a standard curve, then detected the content of polysaccharides, polyphenols, flavonoids, triterpenoid and amino acids.

3.4 Results

3.4.1 PCA Analysis

In the PCA plot, each sample within its respective group is represented as a circle, depicting the differentiation between samples through their clustering or separation patterns. A compact clustering of circle points indicates greater similarity among the observed variables, while a broader dispersion suggests more pronounced differences. Figures 8 and 9 present PCA plots illustrating sample relationships in both positive and negative ion modes. In both ion modes, distinct separation among sample groups is observed, rendering them suitable for metabolome bioinformatics analysis.

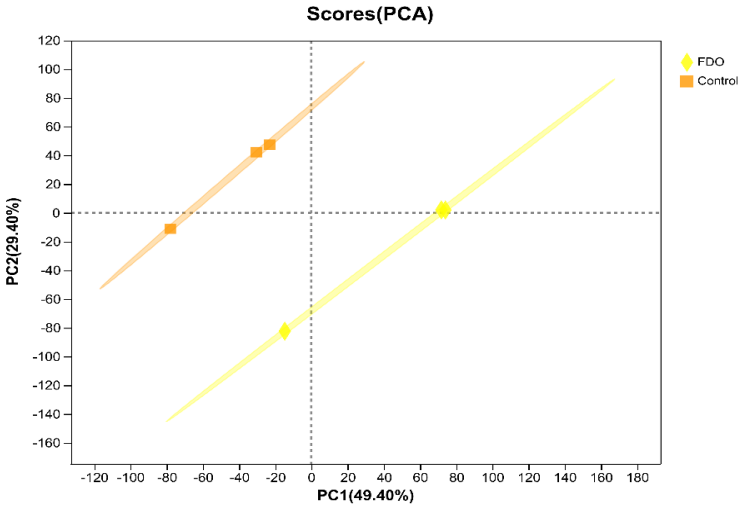

Figure 8. The PCA map of positive ion pattern.

Note: FDO: *D. officinale* fermented by *L. plantarum* GT-17F. Control: *D. officinale.*

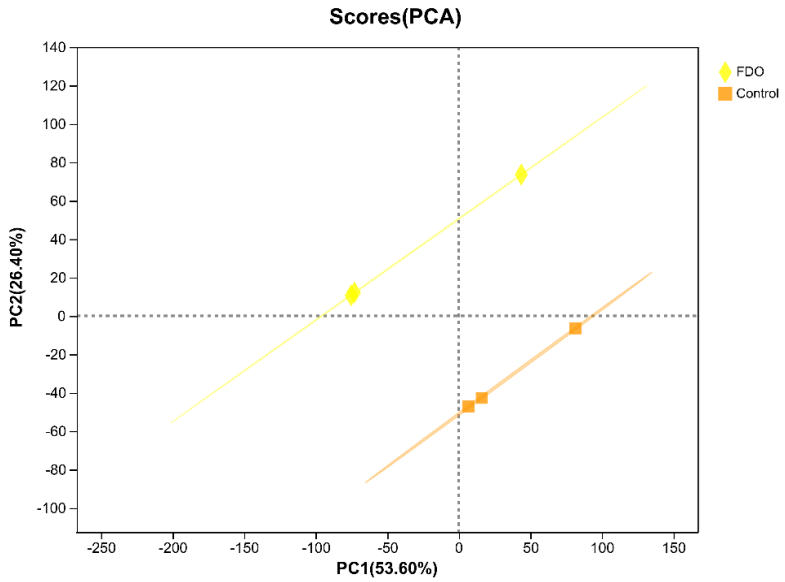

Figure 9. The PCA map of negative ion pattern.

Note: FDO: *D. officinale* fermented by *L. plantarum* GT-17F. Control: *D. officinale.*

3.4.2 Univariate analysis of differential metabolites

We employed volcano plots to visualize the univariate analysis of differential metabolites between *D. officinale* fermentation GT-17F extract (FDO) and *D. officinale* extract (DO=Control). Univariate analysis serves to visually assess the significance of metabolite changes between the two samples, facilitating the identification of potential marker metabolites. The screening criteria were defined as follows: ① p-value ≤ 0.05; ② VIP≥1, with each point representing a metabolite. The positive and negative ion mode data reveal substantial differences in metabolite changes between the two groups (Figure 10).

After conducting univariate and KEGG enrichment analyses on the identified differential metabolites, we identified two groups of key metabolites with biological significance based on differential fold and p-values. Among these, 148 metabolites were up-regulated, while 46 were down-regulated (Appendix Table S). By setting the fold change (FC) (FDO/Control) to ≥1.5 or ≤0.5, we identified a significantly higher number of differentially expressed metabolites. A total of 15 secondary metabolites were

screened and are presented in Table 9. Following *D. officinale* fermentation, we observed 13 up-regulated metabolites, primarily amino acids, acids, lipids, ketones, and glycosides, displaying a significant increase. Additionally, two down-regulated metabolites, mainly olefins and acidic amino acids, exhibited significant reductions.

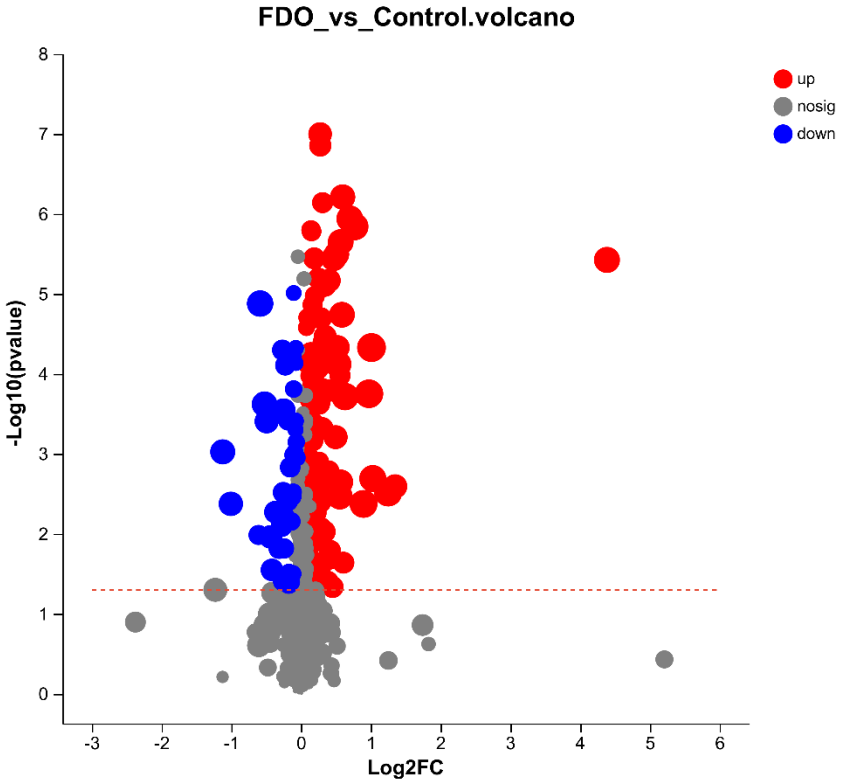

Figure 10. Volcanic map of ion model in FDO and Control (DO).

Note: The horizontal coordinate is the fold change value of the metabolite expression difference between the two groups, namely log2FC; the vertical coordinate is the statistical test value of the metabolite expression difference, namely -log10(p value) value. The higher the value, the more significant the expression difference. Each dot in the figure represents a specific metabolite, and the size of the dot indicates the VIP value. The points on the left are metabolites with differentially down-regulated expression, and the points on the right are metabolites with differentially up-regulated expression. The more the points on the left, right and upper sides, the more significant the expression difference. The corresponding data are shown in the difference details Appendix Table S.

Table 9. Screening results of differential metabolites.

Metab ID	Metabolite	VIP	FC(FDO/Control)	P value
metab_6613	16-Ketoestradiol	2.88	20.89	3.76E-06
metab_15650	Lucidenic acid K	2.47	2.55	0.002549
metab_6005	Tolfenamic acid	3.35	2.38	0.003038
metab_3457	Anisodamine	3.10	2.04	0.002035
metab_11108	5-L-Glutamyl-L-alanine	3.50	2.01	4.69E-05
metab_6851	Madlongiside C	3.49	1.96	0.000177
metab_7473	Norketamine	3.30	1.86	0.004225
metab_6801	Caproic acid	3.19	1.71	1.44E-06
metab_8859	Glycyl-Lysine	3.03	1.62	1.15E-06
metab_18852	Allithiamine	3.18	1.55	0.000192
metab_6922	(S)-Oleuropeic acid	2.03	1.52	0.02293
metab_8418	L-N2-(2-Carboxyethyl) arginine	2.73	1.51	6.16E-07
metab_3551	Agavoside A	2.83	1.50	1.82E-05
metab_15268	11-dehydro-TXB3	2.53	0.50	0.004216
metab_15233	Cofaryloside	2.65	0.46	0.000943

3.4.3 Univariate analysis of differential metabolites

Figure 11 illustrates the key metabolic pathways of *D. officinale* during the fermentation process. The figure reveals that several amino acid biosynthetic pathways undergo the most substantial changes, exerting a primary impact on the metabolic profile. Notably, the secondary pyrimidine metabolic pathway emerges as a crucial aspect of the secondary metabolism in fermented plants. Furthermore, fermentation induces the accumulation of metabolites in pathways associated with carbohydrate metabolism, organic acid metabolism, and glutathione biosynthesis.

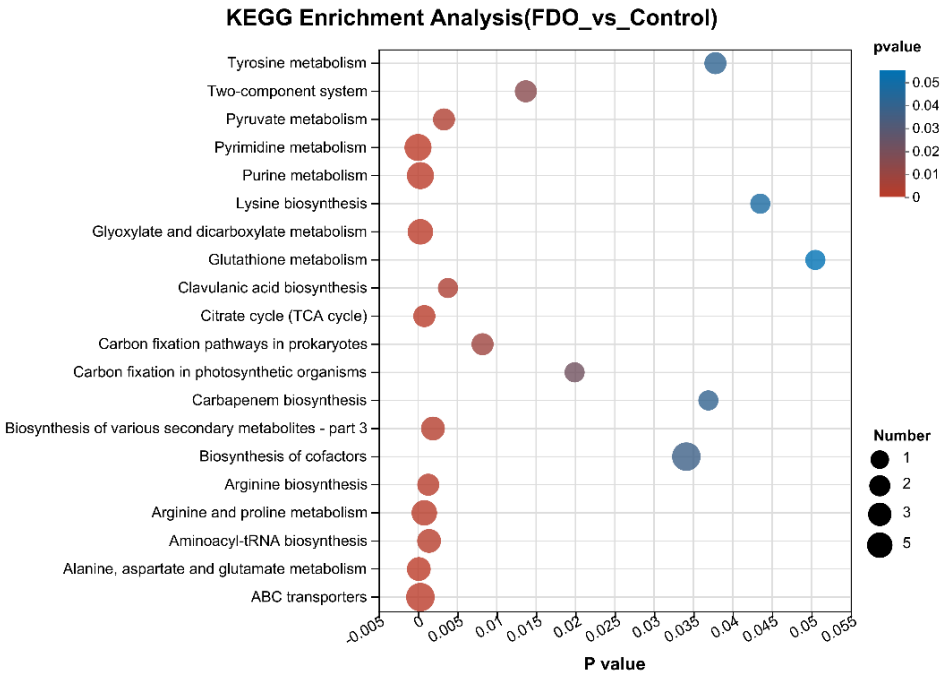

Figure 11. Metabolic pathway analysis.

Note: The horizontal coordinate is the enrichment significance p value, the smaller the p value, the more significant it is statistically. Generally, the p value less than 0.05 is considered as a significant enrichment item. The ordinate is the KEGG pathway. The size of the bubbles in the figure represents how much compound is enriched into the metabolic set in this pathway.

3.4.4 Univariate analysis of differential metabolites

Polysaccharide was the main active ingredient in the extract of *D.officinale* and the extract of *D. officinale* fermented by *L. plantarum* GT-17F. The content of polysaccharide in FDO and DO was 59.16% and 64.97%, respectively. In brief, all the active substances decreased to a certain extent, but the amino acid content increased, which may be due to the fragmentation of the lysate of some *Lactobacillus* and the exudation of intracellular proteins and peptides, leading to the increase of amino acid content (Table10).

Table 10. Contents of each active substance in FDO and DO.

Parameters	FDO (%)	DO (%)
Polyphenol	6.151±0.658	7.534±0.557
Flavone	4.461±0.500	5.923±0.930
Triterpene	0.918±0.025	0.951±0.083
Amino acid	5.5±0.507	7.53±0.38
Polysaccharide	59.16±1.28	64.97±3.11

3.5 Discussion

In recent years, there has been a growing interest in the fermentation of traditional Chinese medicines. However, there is a limited number of reports on metabolomic studies focused on the fermentation of *D. officinale* using *L. plantarum*. This study employs LC-MC metabolomics technology to investigate the metabolomic changes associated with *D. officinale* fermentation. The research aims to analyze the alterations in the metabolic profile and explore the relevant metabolic pathways in *D. officinale* before and after fermentation.

In this study, we conducted a metabolomics analysis of *D. officinale* fermented by *L. plantarum* GT-17F. We established multivariate statistical models, including Principal Component Analysis (PCA) and volcano plot analysis, for comprehensive metabolite profiling. PCA is a technique that reduces the dimensionality of data, transforming multiple variables into a few principal components. In the volcano plot, each point represents a metabolite and illustrates differential metabolites among different groups[53]. Compared to the control group of *D. officinale*, the *D. officinale* fermentation group exhibited 13 up-regulated metabolites and 2 down-regulated metabolites. Notably, there was a significant increase in metabolites such as amino acids, lipids, and ketones, whereas other metabolites, particularly certain amino acids, exhibited a decrease. The key metabolites primarily include 16-ketoestradiol, lucidenic acid K, tolfenamic acid, anisodamine, 5-L-glutamyl-L-alanine, madlongiside C, among

others. These identified metabolites are involved in metabolic pathways including pyruvate metabolism, propionate metabolism, and galactose metabolism[54–56]. The results of this study demonstrate that the metabolite profile of *D. officinale* undergoes significant changes after fermentation by *L. plantarum* GT-17F, diverging notably from unfermented *D. officinale*. This transformation is attributed to the enzymatic activity during *L. plantarum* fermentation, producing extracellular enzymes that break down plant cell walls, increasing intercellular space.

Fermentation can precipitate medicinal components and metabolites in *D. officinale*, resulting in an increase in the content of certain metabolites. Compared to unfermented *D. officinale*, this study convincingly demonstrates significant differences in the metabolite profiles of fermented *D. officinale* through the application of metabolomics technology. During the fermentation process, the choice of different probiotics can impact metabolic pathways and consequently influence the content of active components in *D. officinale*. Variations in metabolic pathways play a pivotal role in determining the differences in metabolites post-fermentation[57]. Distinct metabolic pathways can also exert specific effects on the proliferation of probiotics during the fermentation process. The proliferation of different probiotics, in turn, contributes to variations in metabolites, and their interactions collectively result in the increase or decrease of fermentation metabolites[58]. Currently, most theoretical research on fermented traditional medicine primarily focuses on the determination of probiotics, organic acids, and medicinal components post-fermentation. There is a relative scarcity of research on the mechanisms underlying fermented traditional medicine. This study lays the foundation for future investigations into the interaction mechanisms and clinical applications of fermented *D. officinale*.

Chapter4

Dendrobium officinale extract fermented with a plant-derived lactic acid bacterium enhances the protection effect on UV-mediated skin photoaging

4.1 Introduction

Skin aging caused by ultraviolet radiation (UV radiation) is also called photoaging[59]. Skin aging is primarily attributed to photoaging, which accounts for over 80% of facial aging[60]. Unlike genetically-induced skin aging, photoaged skin experiences a decline in keratinocyte activity within the epidermal layer, leading to a slower renewal rate and weakened epidermal barrier function. Consequently, the skin becomes dry and prone to peeling[61]. The quantity of fibroblasts in the dermis decreases, leading to a deceleration in the synthesis of collagen and elastin, and an acceleration in their decomposition[62]. In photoaged skin, the dermis tissue shows a significant buildup of amorphous elastic fibers, which is the key histological distinction from naturally aged skin. Additionally, there are noticeable irregularities and fractures in collagen fibers, as documented in references[63, 64]. In addition to the aesthetic decline of aging skin, its function of defense against damage is also significantly impaired: after excessive UV irradiation, the integrity of the skin barrier is destroyed, the sebum secretion function is significantly decreased, and the risk of skin inflammation and even skin cancer is significantly increased[65]. UV irradiation will produce abundant ROS, and ROS can undergo the lipid peroxidation reaction with the unsaturated fatty acid chain in vivo to form peroxidized lipids[66, 67]. On the one hand, peroxidized lipids disturb the structure of the phospholipid bilayer and affect the integrity of the cell membrane. Prolonged exposure to UV radiation will result in considerable harm to the dermis' extracellular matrix (ECM)[68]. Collagen, elastin, and glycosaminoglycan are the primary components of dermal ECM, playing a crucial role in preserving the skin's

firmness, elasticity, and moisture[69]. The skin's rough, lax, and creased appearance resulting from photoaging is strongly linked to the elevated levels of MMPs in the skin. MMPs, also known as matrix metalloproteinases, are a group of endopeptidases that rely on zinc for their function. Their primary function in the ECM is to break down different protein components[70]. In skin that has undergone photoaging, there is an increase in the expression of MMPs and a decrease in the expression of their antagonist, TIMPs (tissue inhibitor of matrix metalloproteinases)[71, 72].

Furthermore, *Lactobacillus* can effectively decrease the amount of ROS caused by UV radiation, while also exerting control over the expression of MMPs in skin cells through its impact on various signaling pathways. This regulation leads to a reduction in the breakdown of collagen and elastin following exposure to UV irradiation[73]. It was shown that *L. plantarum* HY7714 effectively decreased the elevated level of MMP-13 transcripts and suppressed the activities of MMP-2 and MMP-9 in cells damaged by UVB. This was achieved by inhibiting the activation of the JNK/AP-1 signaling pathway, as reported by KIM *et al*[74]. The anti-aging properties of *Lactobacillus* have been confirmed not just in cells, but also in animals. It was discovered that hairless mice can effectively combat skin damage from UV radiation by consuming *Bifidum breve* Yakult orally. This is evident through a reduction in elastase activity in the skin and a notable improvement in skin elasticity, unlike mice who did not consume probiotics[75]. Fermentation of other plants by lactic acid bacteria can improve the anti-photoaging activity of natural products. Kang *et al.* discovered that extracts derived from plants fermented with *Lactobacillus* brucei in kimchi were able to effectively hinder the activity of elastase induced by UVB and the expression of MMPs, while also promoting the production of type I procollagen[76]. Utilizing *L. plantarum* GT-17F that is a strain with exceptional antioxidant capabilities identified in previous laboratory research, this investigation opted for conditions that closely resemble natural settings. Fibroblasts subjected to combined UVA and UVB damage, alongside a synthesized skin model, were utilized to evaluate the application prospects of this bacterial strain in formulating skincare products targeting photoaging and photodamage.

4.2 Materials

D. officinale fermented by *L. plantarum* GT-17F (FDO) and unfermented *D. officinale* (DO) were used in the study. Human skin fibroblast (HSF) cells were from Cell Bank/Stem Cell Bank, Chinese Academy of Sciences. EpiSkin™ Reconstructed Human Epidermis and T-Skin™ Human Full Thickness Model were procured from Shanghai Episkin Biotechnology Co., Ltd., Dulbecco's modified Eagle's medium (DMEM), fetal bovine serum (FBS), and penicillin-streptomycin antibiotics were purchased from GIBCO Life Technologies Company. The Cell Counting Kit 8 (CCK-8), reactive oxygen species (ROS) detection kit, Phosphate-buffered saline (PBS), and Hematoxylin and Eosin (HE) Staining Kit were purchased from Beyotime Biotech Inc. Human collagen Type I ELISA kit and human collagen Type III ELISA kit were sourced from Elabscience Biotechnology Co., Ltd. Antibodies for Filaggrin, Loricrin, human collagen Type I, anti-mouse or anti-rabbit secondary antibody, bovine serum albumin, and 4',6-diamidino-2-phenylindole (DAPI) were purchased from Abcam.

4.3 Methods

4.3.1 HSF Cell, EpiSkin™ and T-Skin™ culture

Human skin fibroblasts (HSF) were cultured in DMEM supplemented with 10% FBS and 1% penicillin-streptomycin, incubated at 37°C in a 5% CO_2 atmosphere. EpiSkin™ and T-Skin™ were placed in 12-well plates with 5 mL maintenance medium and incubated at 37°C in 5% CO_2. The next day, the medium was replaced with 2 mL of treatment medium as per EpiSkin 's manual.

4.3.2 Cell Viability Assay of HSF

Cytotoxicity was assessed using a CCK-8 kit according to manufacturer's instructions. Briefly, HSF cells at 1.8×10^5 cells/mL were seeded in 96-well plates and treated with FDO and DO samples for 24 h. Then, 10 μL of CCK-8 solution was added to each well, followed by incubation for 1 h. The absorbance at 450nm was measured, determining cell viability relative to untreated controls[77].

4.3.3 UV Irradiation Procedure

After a 24h incubation with FDO and DO samples, HSF cells and EpiSkin™ were exposed to UVA irradiation at 4J/cm^2 and UVB irradiation at 20mJ/cm^2[78]. The UV source was positioned 15 cm away from the samples, with radiometers ensuring precise irradiation dosage. After irradiation, cells and EpiSkin™ were incubated in complete medium, with or without FDO and DO, for further analysis.

4.3.4 Measurement of Reactive Oxygen Species (ROS)

To evaluate the intracellular generation of reactive oxygen species (ROS), we utilized the oxidation measurement of the probe 2',7'-dichlorofluorescin diacetate (DCFH-DA). In a concise procedure, 6-well culture plates underwent UV damage treatment and were subsequently cultured for 24 h. Following this, 2 mL/well of 2',7'-dichlorofluorescin diacetate (DCFH-DA) at a concentration of 10 μM was introduced to the established cells, with an incubation period of 20 minutes. Fluorescence intensity of the samples was quantified using a fluorescence microplate reader, recording measurements at 495 nm excitation and 545 nm emission wavelengths.

4.3.5 Collagen Production Assessment of HSF and T-Skin™

In this study, 6-well culture plates underwent UV damage treatment and were cultured for 24 h. The levels of collagen type I and III in supernatant culture medium were quantified using ELISA as per the Elabscience 's manual. Absorbance values were measured at 460 nm using a microplate reader, and collagen content was determined based on standard curves.

T-Skin™ Human Full Thickness Model treated with UV damage and cultured for 3 days, immunohistochemistry (IHC) was employed to assess the expression of type I collagen in skin tissues. Frozen sections were processed, blocked with PBS containing 10% bovine serum albumin for 1 h at room temperature, and subjected to overnight incubation with primary antibodies (1:100–1:500) at 4℃. Subsequent steps included PBS washing three times for 10 minutes each, application of fluorescently labeled secondary antibodies (1:200) with an incubation period at 37°C for 1 h, and final PBS

washing three times for 10 minutes each. Slides were sealed after applying the anti-fluorescence quenching agent, and results were observed and photographed using a fluorescence microscope.

4.3.6 Assessment of Skin Barrier Repair

EpiSkin™ Reconstructed Human Epidermis were subjected to UV damage and cultured for a duration of 3 days, then fixed overnight in 4% paraformaldehyde at 4°C. Subsequently, the EpiSkin™ was separated from the basement membrane using a surgical scalpel and socked in PBS for 5 minutes. Tissues underwent dehydration using graded ethanol, vitrification by xylene, and embedding in paraffin. Slices with a thickness of 5μm were obtained from the embedded tissues and processed for hematoxylin and eosin (HE) staining followed by microscopic examination. IHC was employed to examine the expression of FLG and LOR in EpiSkin™. The results were observed and captured using a fluorescence microscope. This comprehensive description employs distinct narrative methods, ensuring clarity and avoiding direct overlap with existing articles[77, 78].

4.3.7 Statistical Analysis

two-way ANOVA was used for statistical comparison between control and experimental groups. Data are reported as mean ± standard error of the mean (SEM). Significance levels were set at an alpha of $\alpha=0.05$. Statistical analyses were considered significant at $\alpha=0.05$. Statistical analysis and graphical representation of data were conducted using GraphPad Prism version 9.

4.4 Results

4.4.1 Comparative Analysis of DO and FDO on HSF Cell Survival

The evaluation of cytotoxicity and protective effects of FDO and DO on HSF cells under UV irradiation utilized a CCK8 assay. Figure 12 illustrates that concentrations of 5 mg/mL for both FDO and DO have no toxic effects on cells. A noteworthy increase

in cell activity rate was observed with rising FDO concentrations ($p < 0.001$), indicating a proliferative effect. Significantly, FDO exhibited a higher cell proliferation rate compared to DO at concentrations of 1.25 mg/mL ($p < 0.05$), 2.5 mg/ml ($p < 0.05$), and 5 mg/mL ($p < 0.01$). Post-UV radiation, evident cell damage occurred, and cell viability correlated with increased FDO and DO concentrations. This observation reaffirms that FDO provides superior protective effects, aiding in the recovery from UV-induced damage to HSF cells compared to DO at concentrations from 1.25 mg/mL up to 5 mg/mL. Subsequent tests utilized experimental concentrations of 0.5, 1, and 5 mg/mL.

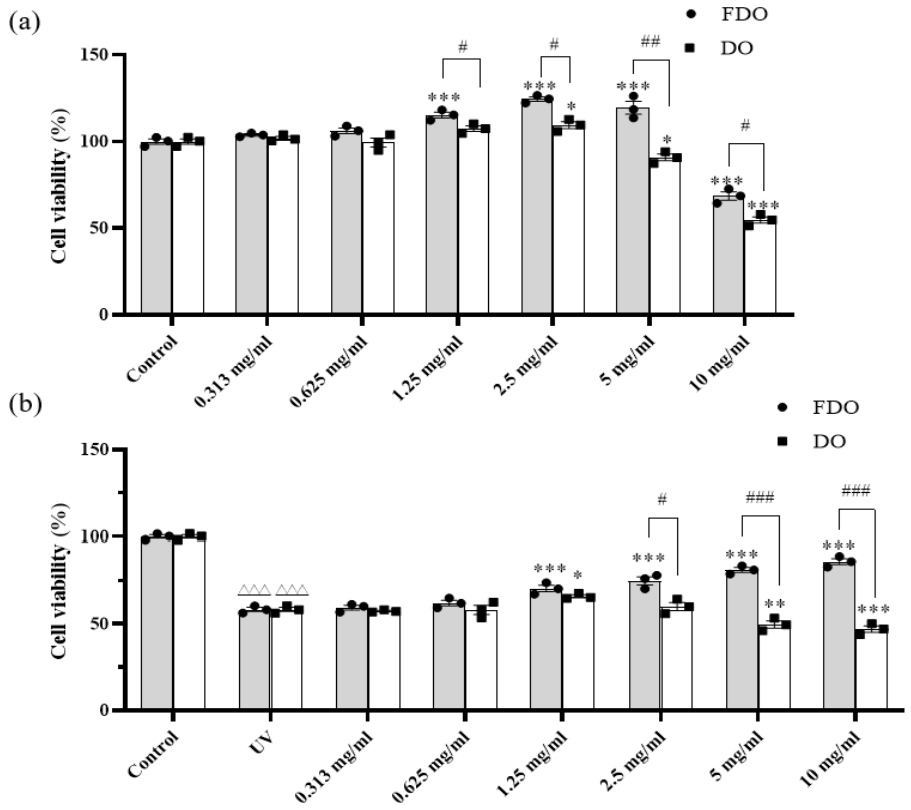

Figure 12. Comparative analysis of FDO and DO on HSF cell survival.

Note: Figure 12 depicts how different concentrations of FDO and DO affect the viability of HSF cells under standard conditions (A) and following exposure to UV radiation (B). Counting results are presented as the mean ± SEM with individual data points, based on three parallel experiments for each group. Statistical analysis utilized ANOVA to assess concentration differences, and a t-test was employed to analyze intergroup differences between FDO and DO groups.

4.4.2 Impact of DO and FDO on ROS Levels in UV- Induced HSF Cells

Effect of DO and DO on UV- induced ROS in HSF was assessed, as depicted in

Figure 13. UV irradiation significantly ($p < 0.05$) increased intracellular ROS accumulation in HSF cells compared to the control (without UV) group. However, pretreatment with FDO, followed by exposure to oxidative stress (+UV), led to a significant ($p < 0.001$) decrease in ROS levels. Specifically, 5 mg/mL FDO pretreatment resulted in a reduction of 63.98%, while 5 mg/mL DO pretreatment showed a decrease of 40.27%. Figure 13 illustrates that FDO exhibits a superior ROS scavenging effect compared to the DO groups, with a significant maximum increase of 158% ($p < 0.001$).

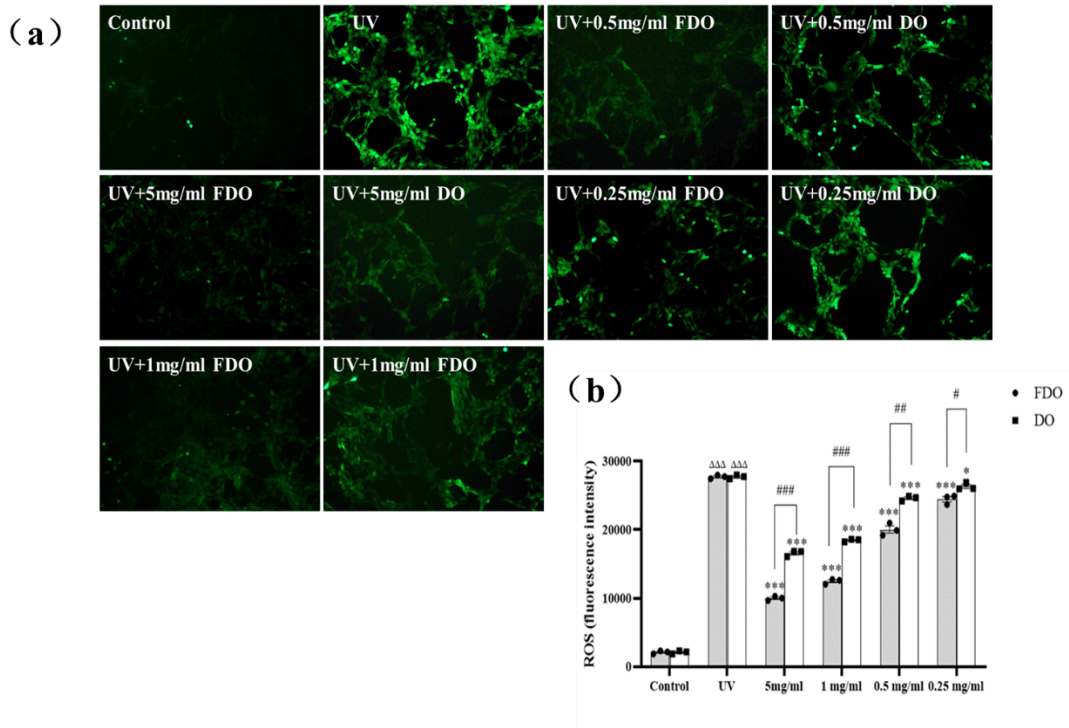

Figure 13. Impact of FDO and DO on ROS levels in UV-irradiated HSF cells.

Note: The group without UV irradiation served as the control. (a) Fluorescence imaging of ROS in HSF cells for each group using an inverted fluorescence microscope. (b) Detection of ROS fluorescence intensity in HSF cells for each group using a fluorescence microplate reader. Counting results are expressed as the mean ± SEM with individual data points, derived from three parallel experiments for each group. Statistical analysis employed ANOVA to evaluate concentration differences, and a t-test was utilized for intergroup comparisons between FDO and DO groups.

4.4.3 Effect of DO and FDO on Collagen Types I and III in UV-induced HSF and T-Skin™ Models

To evaluate the impact of FDO and DO on collagen production in HSF cells and T-Skin™ models subjected to UV radiation, collagen types I and III were quantified

using ELISA techniques. Figure 15 (a, b) illustrates that UV exposure led to a downregulation of both collagen types compared to the control group. Treatment with various concentrations of FDO significantly increased the concentrations of Type I and Type III Collagen in HSF cells compared to the UV-exposed group. At 5 mg/mL pretreatment, FDO significantly increased Type I Collagen by 77.18% ($p < 0.001$), outperforming the 33.97% increase observed with DO. FDO consistently showed superior effects, reaching a maximum 2.27-fold increase compared to DO ($p < 0.001$). This trend persisted with decreasing concentrations, and at 0.5mg/mL, DO exhibited no significant increase in Type I Collagen. Similar patterns were observed for Type III Collagen, with no significant increase in the DO group at 1mg/mL concentration.

The protective effects of UV-induced photoaging effects of 3-day treatment with FDO and DO were tested in T-Skin™ (Figure 15 c, d). Following treatment, a notable decrease in type I Collagen markers was observed compared to control tissues, indicating a significant 54.2% decrease ($p < 0.001$) in type I Collagen expression in UV-mediated T-Skin™. However, FDO and DO treatment (1 mg/mL, 5 mg/mL) led to increased type I Collagen expression in the dermis compared to UV tissues. FDO demonstrated a significant increase of 53% and 93% (both $p < 0.001$), while DO show a significant increase of 130% ($p < 0.01$) at a concentration of 5 mg/mL.

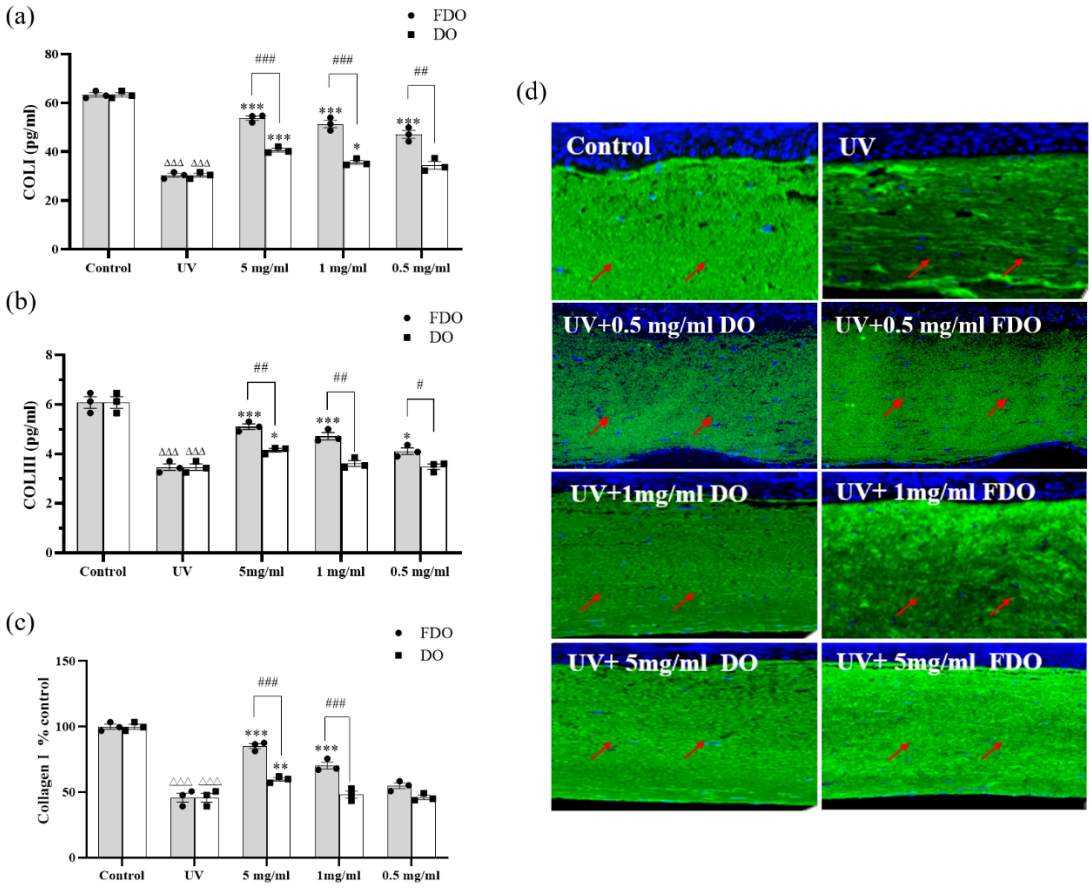

Figure 14. Effect of DO and FDO on collagen Types I and III in UV-irradiated HSF and T-Skin™.

Note: (a) Investigated the impact of DO and FDO on UV-irradiated HSF cells' secretion of type I collagen. (b) Explored the effects of DO and FDO on UV-induced HSF cells' secretion of type III collagen. (c) Detected the immunofluorescence intensity of type I collagen in T-Skin™ slices relative to the Control group. (d) Conducted immunofluorescence imaging of type I collagen in T-Skin™ slices. Counting results are presented as the mean ± SEM with individual data points, based on three parallel experiments for each group. Statistical analysis utilized ANOVA to assess concentration differences, and a t-test was employed to analyze intergroup differences between FDO and DO groups.

4.4.4 Effect of DO and FDO in Repairing UV-Damaged Skin Barrier in EpiSkin™ Models

In the context of skin physiology, UV radiation stands out as a prominent instigator of skin photoaging, inflicting considerable harm on keratinocytes and precipitating a compromised skin barrier characterized by the depletion of filaggrin (FLG) and loricrin (LOR). To scrutinize the impact, EpiSkin™ sections underwent HE staining, enabling the measurement of living layer thickness from meticulously calibrated digital images (Figure 15a)[79, 80]. The study focused on evaluating the skin barrier repair potential

following a 3-day treatment with Fermented *D. officinale* (FDO) and unfermented *D. officinale* (DO) against UV-induced damage in EpiSkin™. The results revealed a significant UV-induced downregulation ($p < 0.001$) in epidermal thickness compared to the control group. However, post-treatment with FDO and DO (1 mg/mL, 5 mg/mL) exhibited a noteworthy increase in epidermal thickness relative to UV-exposed tissues (Figure 15b). Particularly striking was the observation that only FDO at a concentration of 5mg/mL demonstrated a statistically significant improvement ($p < 0.001$) in the thickness of the reconstructed epidermal model. This finding underscores the distinct efficacy of FDO in mitigating UV-induced damage and holds promise for its application in skin health interventions.

UV radiation is a well-known contributor to skin photoaging, causing substantial damage to keratinocytes and resulting in barrier impairment marked by the loss of filaggrin (FLG) and loricrin (LOR). EpiSkin™ sections underwent HE staining, and the thickness of living layers was measured from calibrated digital images (Figure 15a). The skin barrier repair effects of 3 days of treatment with FDO and DO against UV-induced damage were examined in EpiSkin™. UV challenge significantly downregulated ($p < 0.001$) epidermal thickness compared to the control group. However, after treatment with FDO and DO (1 mg/mL, 5 mg/mL), there was an increase in epidermal thickness compared to UV tissues (Figure 15b). Notably, only FDO at a concentration of 5mg/mL significantly improved ($p < 0.001$) the thickness of the reconstructed epidermal model.

To delve into the influence of FDO and DO on barrier-related proteins, specifically filaggrin (FLG) and loricrin (LOR), in UV-mediated EpiSkin™ Reconstructed Human Epidermis, we conducted immunofluorescence analysis (Figure 15c, d). Employing ImageJ for semi-quantitative expression analysis (Figure 15e, f), UV-induced EpiSkin™ exhibited a noteworthy decrease of 38% ($p < 0.001$) and 37% ($p < 0.001$) in FLG and LOR expression, respectively. Subsequent treatment with FDO and DO at concentrations of 1mg/mL or 5mg/mL resulted in a significant upregulation of FLG and LOR expression in the epidermis compared to UV-induced EpiSkin™. Particularly, FDO, at concentrations of 5mg/mL and 1mg/mL, demonstrated a remarkable increase

in FLG expression by 152% ($p < 0.001$) and 139% ($p > 0.001$), respectively. Following DO treatment at 5mg/mL, FLG expression significantly increased by 125% ($p < 0.01$), with no significant difference observed at 1mg/mL. The expression pattern for LOR closely mirrored that of FLG. These findings illuminate the pronounced impact of FDO and DO on restoring FLG and LOR expression in UV-mediated EpiSkin™, underscoring their potential in fortifying the skin barrier against UV-induced damage.

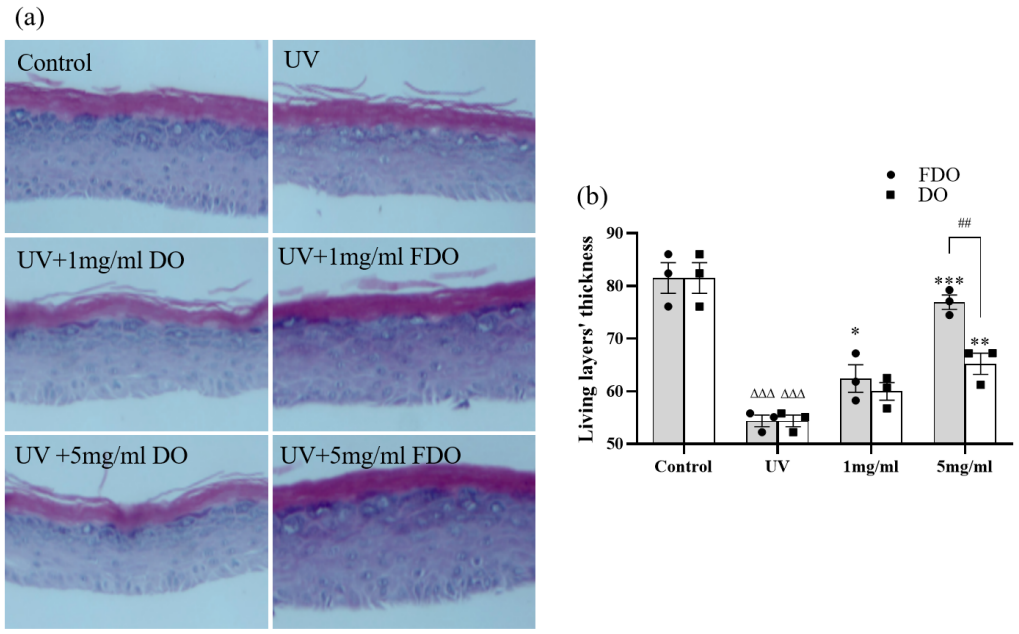

Figure 15. Effect of DO and FDO in repairing UV-damaged skin barrier in EpiSkin™.

Note: (a) HE-stained images of the epidermal thickness of DO and FDO on the EpiSkin™ after UV-damaged. (b) The thickness of the skin model (μm). Counting results are presented as the mean ± SEM with individual data points, based on three parallel experiments for each group. Statistical analysis utilized ANOVA to assess concentration differences, and a t-test was employed to analyze intergroup differences between FDO and DO groups.

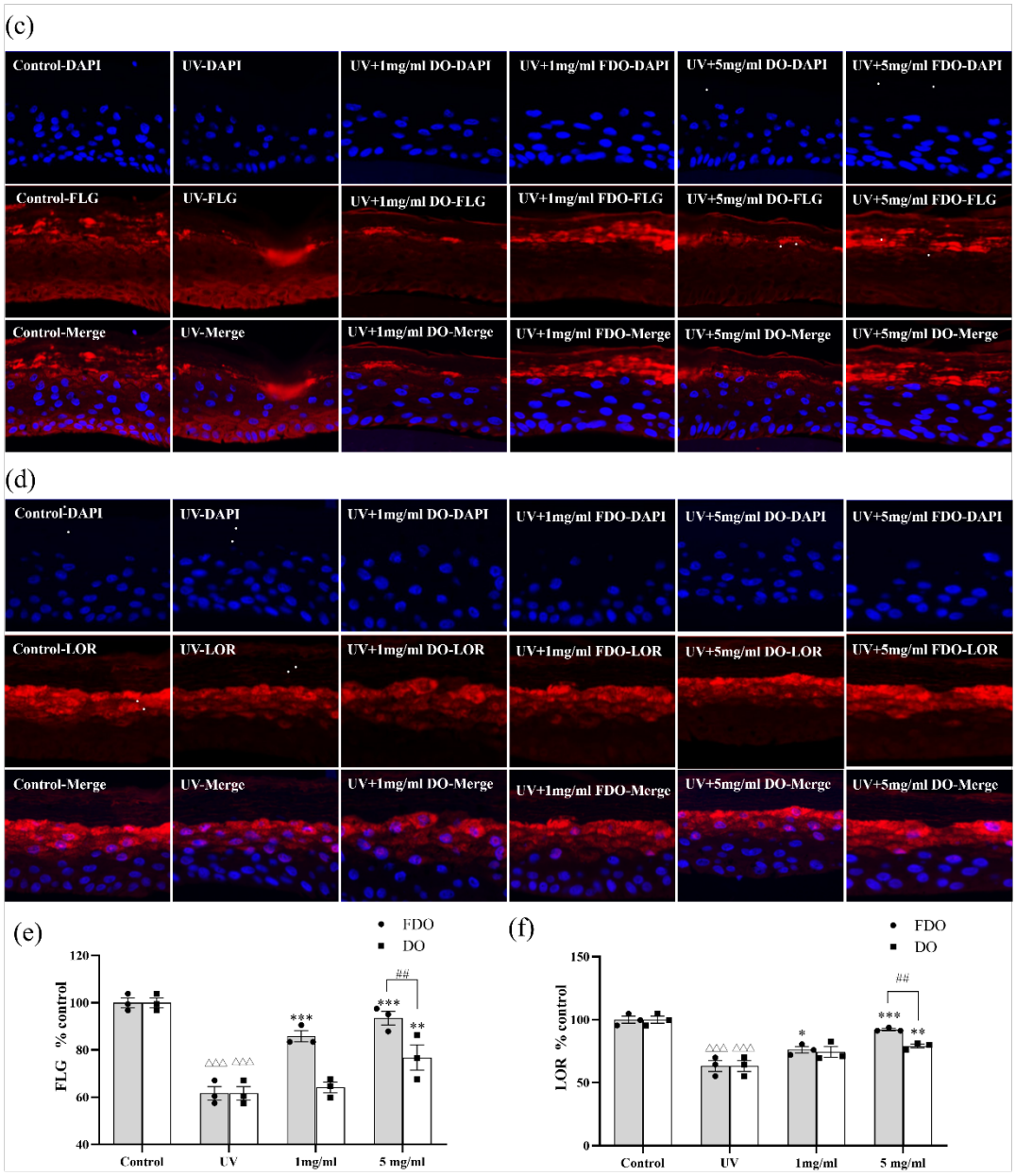

Figure 15. Effect of DO and FDO in repairing UV-damaged skin barrier in EpiSkin™ (Continued).

Note: (c) Immunofluorescence image of FLG expression on the EpiSkin™ model after UV irradiation. (d) Immunofluorescence image of LOR expression on the EpiSkin™ after UV-damaged. (e) Relative intensity statistics of FLG immunofluorescence in EpiSkin™ model, relative to the control group. (f) The relative intensity statistics of LOR immunofluorescence in EpiSkin™ model, relative to the control group. Counting results are presented as the mean ± SEM with individual data points, based on three parallel experiments for each group. Statistical analysis utilized ANOVA to assess concentration differences, and a t-test was employed to analyze intergroup differences between FDO and DO groups.

4.5 Discussion

The vast spectrum of active ingredients, including polysaccharides, flavonoids, polyphenols, and amino acids, inherent in plant raw materials has long been revered for its multifaceted benefits to skin[81]. Despite this acclaim, traditional extraction methods often fall short of expectations, encountering limitations in both process and solvent choices[82]. A paradigm shift towards fermentation of plant raw materials has emerged, demonstrating an ability to enrich effective nutrients and amplify raw material efficacy[83, 84]. This has spurred a growing scientific interest in the amalgamation of Chinese herb extracts and probiotics through fermentation, revolutionizing the landscape of cosmetic plant functional raw materials.

Scientific investigations, including our study, have cast a spotlight on the unique partnership between *D. officinale* (DO) and *L. plantarum*, showcasing superior antioxidative and anti-photoaging effects. Those studies have shown that the combination of *D. officinale* and *L. plantarum* possess better antioxidative and anti-photoaging effects[85]. In our study[86], we delved into the intricate nuances differentiating the anti-photoaging functions of *L. plantarum* GT-17F fermented *D. officinale* (FDO) from its unfermented counterpart (DO). This exploration aimed to dissect how fermentation influences the material's efficacy in countering external factors that precipitate skin photoaging. Acknowledging that external factors, notably ultraviolet (UV) radiation, infrared exposure, chemical smoke, and haze, contribute significantly to skin photoaging, penetrating the epidermal layer to the dermis, inflicting damage upon collagen fibers, instigating skin aging, and the formation of wrinkles[68].

Under normal conditions, the unassuming levels of ROS in HSF cells go unnoticed. However, when exposed to UV radiation, ROS levels soar, subjecting the cells to heightened oxidative stress. The pivotal revelation from our study lies in the post-UV application of FDO and unfermented DO, revealing a concentration-dependent gradient effect on ROS levels. Notably, FDO demonstrates a superior ability to quell ROS, showcasing a widening gap over DO as concentrations rise.

In the intricate domain of skin physiology, fibroblasts in the human dermis play a pivotal role in the generation of the ECM, where collagen integrity stands as a cornerstone for optimal skin function. Our investigation delves into the viability of human skin fibroblast (HSF) cells, revealing a significant disparity—higher concentrations of DO markedly diminish cell viability, potentially due to elevated polysaccharide content and viscosity. This inhibitory effect undergoes a transformative shift post-fermentation, mitigating viscosity and breaking down polysaccharides into oligosaccharides[87]. Additionally, FDO emerges as a defender against UV-induced collagen degradation, displaying unique efficacy in preserving collagen at low doses, a feat not mirrored by unfermented DO.

The EpiSkin™ Reconstructed Human Epidermis consisting of co-cultured normal human epidermal keratinocytes (NHEK) and normal human dermal fibroblasts (NHDF), is derived from neonatal foreskin, offering a differentiated, multilayered simulation of human skin. EpiSkin™ meticulously replicates the organized basal, spinous, granular, and cornified epidermal layers observed *in vivo*[88]. Ultra structurally, the T-Skin™ closely resembles human skin, provided an in vitro model for studying collagen expression in the dermis. These skin models effectively simulate the effects of UV damage on human skin. Exposing these models to UV radiation enables the evaluation of changes in skin thickness and the expression of key epidermal barrier proteins, including FLG and LOR, using HE-staining and immunofluorescence techniques. This approach offers insights into the structural and molecular changes in the skin resulting from UV exposure.

The unfortunate consequence of UV damage, as evidenced by these studies, is a significant structural impact on the skin, resulting in a substantial loss of barrier proteins. Even with interventions utilizing FDO and DO, the full restoration of the initial state remains elusive. However, the scientific evidence indicates that FDO exhibits a superior ability to ameliorate the effects of UV damage compared to DO, suggesting its potential as a more effective skincare agent.

Conclusion

The present study adopts the research direction of the laboratory, the development and research of *L. plantarum* in the field of beauty and health. Different from the development and application of animal-derived *Lactobacillus* in European and American countries, our laboratory is more inclined to develop some plant lactic acid bacilli that are more suitable for the intestinal tract and skin of people in East Asia. At the same time, it is also believed that *L. plantarum* screened from the natural environment, because it is affected by temperature, light, ultraviolet light, and other microbial stress for a long time, compared with the constant temperature of animal source, no ultraviolet light and harmless microbial stress, has greater development value. In this study, the well-known traditional medicine *D. officinale* was taken as the research object, and the *L. plantarum* in its growth environment was screened, to obtain the secondary metabolite *L. plantarum* that can co-exist with it and produce stronger activity.

By screening the symbiotic *L. plantarum* of *D. officinale*, we obtained 23 strains of *L. plantarum*, and studied the antioxidant capacity and fermentation kinetics of 5 strains of *L. plantarum* which were highly enriched. *L. plantarum* GT-17F was selected as the research object, and the fermentation substrate was *D. officinale* juice. The fermentation time was 48 h, and the fermentation temperature was 35±2℃.

It was determined by non-targeted metabolomics analysis and physicochemical methods, through compared with the *D. officinale* group, 13 up-regulated metabolites and 2 down-regulated metabolites were screened out in the *D. officinale* fermentation group. The amino acids, lipids, ketones, and other differential metabolites were significantly increased, and certain amino acids were significantly decreased. The key metabolites are mainly 16-ketoestradiol, lucidenic acid K, tolfenamic acid, anisodamine, 5-L-glutamyl-L-alanine and madlongiside C. Polysaccharide was the main active ingredient in the extract of *D. officinale* and the extract of *D. officinale* fermented with *L. plantarum* GT-17F. The content of polysaccharide in FDO and DO was 59.16% and

64.97%, respectively. Overall, in addition to amino acid content, other components showed a decline, although the decline, such as polysaccharides may be degraded into more reactive oligosaccharides.

This study demonstrates how *L. plantarum* GT-17F fermentation of *D. officinale* enhances protection against UV-mediated photoaging. Our findings indicate that the FDO exhibits enhanced antioxidant activity, particularly in scavenging free radicals. Administering FDO to HSF cells and synthetic skin constructs prior to UV exposure mitigated the breakdown of collagen types I and III, bolstered the integrity of the epidermal barrier, and diminished harm to key barrier proteins, including FLG and LOR. Yet, the precise biochemical transformations in *D. officinale* following fermentation with *L. plantarum* GT-17F are still under investigation. These findings, nonetheless, establish a foundation for subsequent inquiries into the efficacy of fermented *D. officinale* in addressing UV-related skin damage and aging in human applications.

Reference

[1] NADEESHANI DILHARA GAMAGE D G, DHARMADASA R M, CHANDANA ABEYSINGHE D, et al. Global Perspective of Plant-Based Cosmetic Industry and Possible Contribution of Sri Lanka to the Development of Herbal Cosmetics [J]. Evid Based Complement Alternat Med, 2022, 2022: 9940548.

[2] RODRIGUEZ-YOLDI M J. Anti-Inflammatory and Antioxidant Properties of Plant Extracts [J]. Antioxidants (Basel), 2021, 10(6).

[3] VAN WYK A S, PRINSLOO G. Health, safety and quality concerns of plant-based traditional medicines and herbal remedies [J]. South African Journal of Botany, 2020, 133: 54-62.

[4] ZHANG J, ONAKPOYA I J, POSADZKI P, et al. The safety of herbal medicine: from prejudice to evidence [J]. Evid Based Complement Alternat Med, 2015, 2015: 316706.

[5] HEATH R S, RUSCOE R E, TURNER N J. The beauty of biocatalysis: sustainable synthesis of ingredients in cosmetics [J]. Nat Prod Rep, 2022, 39(2): 335-88.

[6] ZIEMLEWSKA A, NIZIOL-LUKASZEWSKA Z, BUJAK T, et al. Effect of fermentation time on the content of bioactive compounds with cosmetic and dermatological properties in Kombucha Yerba Mate extracts [J]. Sci Rep, 2021, 11(1): 18792.

[7] VAN DEN NIEUWBOER M, VAN HEMERT S, CLAASSEN E, et al. *Lactobacillus plantarum* WCFS1 and its host interaction: a dozen years after the genome [J]. Microb Biotechnol, 2016, 9(4): 452-65.

[8] GARCíA-BURGOS M, MORENO-FERNáNDEZ J, ALFéREZ M J M, et al. New perspectives in fermented dairy products and their health relevance [J]. Journal of Functional Foods, 2020, 72: 104059.

[9] ZHANG L, QU H, LIU X, et al. Comparison and selection of probiotic *Lactobacillus* from human intestinal tract and traditional fermented food in vitro via PCA, unsupervised clustering algorithm, and heat-map analysis [J]. Food Sci Nutr, 2022, 10(12): 4247-57.

[10] WIDYASTUTI Y, FEBRISIANTOSA A, TIDONA F. Health-Promoting Properties of Lactobacilli in Fermented Dairy Products [J]. Front Microbiol, 2021, 12: 673890.

[11] VIESSER J A, DE MELO PEREIRA G V, DE CARVALHO NETO D P, et al. Exploring

the contribution of fructophilic lactic acid bacteria to cocoa beans fermentation: Isolation, selection and evaluation [J]. Food Res Int, 2020, 136: 109478.

[12] MICHALAK M. Plant-Derived Antioxidants: Significance in Skin Health and the Ageing Process [J]. Int J Mol Sci, 2022, 23(2).

[13] RICCI A, CIRLINI M, MAOLONI A, et al. Use of Dairy and Plant-Derived Lactobacilli as Starters for Cherry Juice Fermentation [J]. Nutrients, 2019, 11(2).

[14] AYED L, M'HIR S, HAMDI M. Microbiological, Biochemical, and Functional Aspects of Fermented Vegetable and Fruit Beverages [J]. Journal of Chemistry, 2020, 2020: 1-12.

[15] HASHEMI S M B, MOUSAVI KHANEGHAH A, BARBA F J, et al. Fermented sweet lemon juice (Citrus limetta) using *Lactobacillus plantarum* LS5: Chemical composition, antioxidant and antibacterial activities [J]. Journal of Functional Foods, 2017, 38: 409-14.

[16] KUN S, REZESSY-SZABó J M, NGUYEN Q D, et al. Changes of microbial population and some components in carrot juice during fermentation with selected Bifidobacterium strains [J]. Process Biochemistry, 2008, 43(8): 816-21.

[17] MOUSAVI Z, MOUSAVI S M, RAZAVI S H, et al. Effect of Fermentation of Pomegranate Juice by *Lactobacillus plantarum* and *Lactobacillus* acidophilus on the Antioxidant Activity and Metabolism of Sugars, Organic Acids and Phenolic Compounds [J]. Food Biotechnology, 2013, 27: 1 - 13.

[18] XU X, ZHANG C, WANG N, et al. Bioactivities and Mechanism of Actions of *Dendrobium officinale*: A Comprehensive Review [J]. Oxid Med Cell Longev, 2022, 2022: 6293355.

[19] GUO L, QI J, DU D, et al. Current advances of *Dendrobium officinale* polysaccharides in dermatology: a literature review [J]. Pharm Biol, 2020, 58(1): 664-73.

[20] CHEN S, CAO P, LANG F, et al. Adhesion-Related Immunomodulatory Activity of the Screened *Lactobacillus plantarum* from Sichuan Pickle [J]. Curr Microbiol, 2019, 76(1): 29-36.

[21] DOS SANTOS LEANDRO E, GINANI V C, DE ALENCAR E R, et al. Isolation, Identification, and Screening of Lactic Acid Bacteria with Probiotic Potential in Silage of Different Species of Forage Plants, Cocoa Beans, and Artisanal Salami [J]. Probiotics Antimicrob Proteins, 2021, 13(1): 173-86.

[22] MENG F, LYU Y, ZHAO H, et al. LsrR-like protein responds to stress tolerance by

regulating polysaccharide biosynthesis in Lactiplantibacillus plantarum [J]. Int J Biol Macromol, 2023, 225: 1193-203.

[23] GAGGIA F, DI GIOIA D, BAFFONI L, et al. The role of protective and probiotic cultures in food and feed and their impact in food safety [J]. Trends in Food Science & Technology, 2011, 22: S58-S66.

[24] JIANG J, SHI B, ZHU D, et al. Characterization of a novel bacteriocin produced by *Lactobacillus* sakei LSJ618 isolated from traditional Chinese fermented radish [J]. Food Control, 2012, 23(2): 338-44.

[25] KHAN H, FLINT S, YU P L. Enterocins in food preservation [J]. Int J Food Microbiol, 2010, 141(1-2): 1-10.

[26] TAMANG J P, TAMANG B, SCHILLINGER U, et al. Functional properties of lactic acid bacteria isolated from ethnic fermented vegetables of the Himalayas [J]. Int J Food Microbiol, 2009, 135(1): 28-33.

[27] ŠUŠKOVIĆ J, KOS B, BEGANOVIĆ J, et al. Antimicrobial Activity – The Most Important Property of Probiotic and Starter Lactic Acid Bacteria [J]. Food Technology and Biotechnology, 2010, 48: 296-307.

[28] SZUTOWSKA J. Functional properties of lactic acid bacteria in fermented fruit and vegetable juices: a systematic literature review [J]. European Food Research and Technology, 2020, 246(3): 357-72.

[29] DARBANDI A, ASADI A, MAHDIZADE ARI M, et al. Bacteriocins: Properties and potential use as antimicrobials [J]. J Clin Lab Anal, 2022, 36(1): e24093.

[30] MANTZOURANI I, BONTSIDIS C A, PLESSAS S, et al. Comparative Susceptibility Study Against Pathogens Using Fermented Cranberry Juice and Antibiotics [J]. Front Microbiol, 2019, 10: 1294.

[31] GUSTAW K, NIEDŹWIEDŹ I, RACHWAŁ K, et al. New Insight into Bacterial Interaction with the Matrix of Plant-Based Fermented Foods [J]. Foods, 2021, 10(7): 1603.

[32] HUR S J, LEE S Y, KIM Y-C, et al. Effect of fermentation on the antioxidant activity in plant-based foods [J]. Food Chemistry, 2014, 160: 346-56.

[33] ZHAO M, ZHANG F, ZHANG L, et al. Mixed fermentation of jujube juice (Ziziphus jujuba Mill.) with L. rhamnosus GG and *L. plantarum* -1: effects on the quality and stability

[J]. International Journal of Food Science & Technology, 2019.

[34] PAN X, ZHANG S, XU X, et al. Volatile and non-volatile profiles in jujube pulp co-fermented with lactic acid bacteria [J]. LWT, 2022, 154: 112772.

[35] LEONARD W, ZHANG P, YING D, et al. Fermentation transforms the phenolic profiles and bioactivities of plant-based foods [J]. Biotechnol Adv, 2021, 49: 107763.

[36] LEE H-Y, PARK J-H, SEOK S-H, et al. Human originated bacteria, *Lactobacillus* rhamnosus PL60, produce conjugated linoleic acid and show anti-obesity effects in diet-induced obese mice [J]. Biochimica et Biophysica Acta (BBA) - Molecular and Cell Biology of Lipids, 2006, 1761(7): 736-44.

[37] VAN DER STRAATEN T, ZULIANELLO L, VAN DIEPEN A, et al. Salmonella enterica serovar Typhimurium RamA, intracellular oxidative stress response, and bacterial virulence [J]. Infect Immun, 2004, 72(2): 996-1003.

[38] KIM H S, CHAE H S, JEONG S G, et al. Antioxidant Activity of Some Yogurt Starter Cultures [J]. Asian-Australas J Anim Sci, 2005, 18(2): 255-8.

[39] SPYROPOULOS B G, MISIAKOS E P, FOTIADIS C, et al. Antioxidant properties of probiotics and their protective effects in the pathogenesis of radiation-induced enteritis and colitis [J]. Dig Dis Sci, 2011, 56(2): 285-94.

[40] VERóN H E, GAUFFIN CANO P, FABERSANI E, et al. Cactus pear (Opuntia ficus-indica) juice fermented with autochthonous *Lactobacillus plantarum* S-811 [J]. Food Funct, 2019, 10(2): 1085-97.

[41] SEPTEMBRE-MALATERRE A, REMIZE F, POUCHERET P. Fruits and vegetables, as a source of nutritional compounds and phytochemicals: Changes in bioactive compounds during lactic fermentation [J]. Food Research International, 2018, 104: 86-99.

[42] TAMANG J P, WATANABE K, HOLZAPFEL W H. Review: Diversity of Microorganisms in Global Fermented Foods and Beverages [J]. Front Microbiol, 2016, 7: 377.

[43] WANG X, ZHOU X, WANG K, et al. Structural characterisation and bioactivity of polysaccharides isolated from fermented *Dendrobium officinale* [J]. J Sci Food Agric, 2022, 102(1): 280-90.

[44] LIU Y, CHENG H, LIU H, et al. Fermentation by Multiple Bacterial Strains Improves the Production of Bioactive Compounds and Antioxidant Activity of Goji Juice [J]. Molecules,

2019, 24(19).

[45] HU Y, ZHANG L, WEN R, et al. Role of lactic acid bacteria in flavor development in traditional Chinese fermented foods: A review [J]. Crit Rev Food Sci Nutr, 2022, 62(10): 2741-55.

[46] BROWN D G, BORRESEN E C, BROWN R J, et al. Heat-stabilised rice bran consumption by colorectal cancer survivors modulates stool metabolite profiles and metabolic networks: a randomised controlled trial [J]. Br J Nutr, 2017, 117(9): 1244-56.

[47] NICHOLSON J K, LINDON J C, HOLMES E. 'Metabonomics': understanding the metabolic responses of living systems to pathophysiological stimuli via multivariate statistical analysis of biological NMR spectroscopic data [J]. Xenobiotica, 1999, 29(11): 1181-9.

[48] PATEL M K, PANDEY S, KUMAR M, et al. Plants Metabolome Study: Emerging Tools and Techniques [J]. Plants (Basel), 2021, 10(11).

[49] NIU Y, WANG H, XIE Z, et al. Structural analysis and bioactivity of a polysaccharide from the roots of Astragalus membranaceus (Fisch) Bge. var. mongolicus (Bge.) Hsiao [J]. Food Chemistry, 2011, 128(3): 620-6.

[50] ZHANG J, CHEN G, ZHAO P, et al. The abundance of certain metabolites responds to drought stress in the highly drought tolerant plant Caragana korshinskii [J]. Acta Physiologiae Plantarum, 2017, 39(5): 116.

[51] PATTI G J, YANES O, SIUZDAK G. Innovation: Metabolomics: the apogee of the omics trilogy [J]. Nat Rev Mol Cell Biol, 2012, 13(4): 263-9.

[52] PLUMB R S, GRANGER J H, STUMPF C L, et al. A rapid screening approach to metabonomics using UPLC and oa-TOF mass spectrometry: application to age, gender and diurnal variation in normal/Zucker obese rats and black, white and nude mice [J]. Analyst, 2005, 130(6): 844-9.

[53] WERTH M T, HALOUSKA S, SHORTRIDGE M D, et al. Analysis of metabolomic PCA data using tree diagrams [J]. Anal Biochem, 2010, 399(1): 58-63.

[54] HENRIQUEZ S, KOHEN P, XU X, et al. Estrogen metabolites in human corpus luteum physiology: differential effects on angiogenic activity [J]. Fertil Steril, 2016, 106(1): 230-7 e1.

[55] HENRIQUEZ S, KOHEN P, XU X, et al. Significance of pro-angiogenic estrogen metabolites in normal follicular development and follicular growth arrest in polycystic ovary syndrome [J]. Hum Reprod, 2020, 35(7): 1655-65.

[56] EMOND J P, LACOMBE L A-O, CARON P, et al. Urinary oestrogen steroidome as an indicator of the risk of localised prostate cancer progression [J]. (1532-1827 (Electronic)).

[57] WANG Z, JIN X, ZHANG X, et al. From Function to Metabolome: Metabolomic Analysis Reveals the Effect of Probiotic Fermentation on the Chemical Compositions and Biological Activities of Perilla frutescens Leaves [J]. Front Nutr, 2022, 9: 933193.

[58] YUAN Y, YANG Y, XIAO L, et al. Advancing Insights into Probiotics during Vegetable Fermentation. LID - 10.3390/foods12203789 [doi] LID - 3789 [J]. (2304-8158 (Print)).

[59] CAVINATO M, JANSEN-DüRR P. Molecular mechanisms of UVB-induced senescence of dermal fibroblasts and its relevance for photoaging of the human skin [J]. Exp Gerontol, 2017, 94: 78-82.

[60] FRIEDMAN O. Changes associated with the aging face [J]. Facial Plast Surg Clin North Am, 2005, 13(3): 371-80.

[61] KWON O S, YOO H G, HAN J H, et al. Photoaging-associated changes in epidermal proliferative cell fractions in vivo [J]. Arch Dermatol Res, 2008, 300(1): 47-52.

[62] FARAGE M A, MILLER K W, ELSNER P, et al. Characteristics of the Aging Skin [J]. Adv Wound Care (New Rochelle), 2013, 2(1): 5-10.

[63] VARANI J, SCHUGER L, DAME M K, et al. Reduced Fibroblast Interaction with Intact Collagen as a Mechanism for Depressed Collagen Synthesis in Photodamaged Skin [J]. Journal of Investigative Dermatology, 2004, 122(6): 1471-9.

[64] ZAWROTNIAK M, BARTNICKA D, RAPALA-KOZIK M. UVA and UVB radiation induce the formation of neutrophil extracellular traps by human polymorphonuclear cells [J]. J Photochem Photobiol B, 2019, 196: 111511.

[65] PILLAI S, ORESAJO C, HAYWARD J. Ultraviolet radiation and skin aging: roles of reactive oxygen species, inflammation and protease activation, and strategies for prevention of inflammation-induced matrix degradation - a review [J]. Int J Cosmet Sci, 2005, 27(1): 17-34.

[66] NIKI E. Lipid oxidation in the skin [J]. Free Radic Res, 2015, 49(7): 827-34.

[67] DE JAGER T L, COCKRELL A E, DU PLESSIS S S. Ultraviolet Light Induced Generation of Reactive Oxygen Species [J]. Adv Exp Med Biol, 2017, 996: 15-23.

[68] WATSON R E, GIBBS N K, GRIFFITHS C E, et al. Damage to skin extracellular matrix induced by UV exposure [J]. Antioxid Redox Signal, 2014, 21(7): 1063-77.

[69] OXLUND H, ANDREASSEN T T. The roles of hyaluronic acid, collagen and elastin in the mechanical properties of connective tissues [J]. J Anat, 1980, 131(Pt 4): 611-20.

[70] BIRKEDAL-HANSEN H. [8] Catabolism and turnover of collagens: Collagenases [M]. Methods in Enzymology. Academic Press. 1987: 140-71.

[71] LEPHART E D, SOMMERFELDT J M, ANDRUS M B. Resveratrol: influences on gene expression in human skin [J]. Journal of Functional Foods, 2014, 10: 377-84.

[72] AFAQ F, KATIYAR S K. Polyphenols: skin photoprotection and inhibition of photocarcinogenesis [J]. Mini Rev Med Chem, 2011, 11(14): 1200-15.

[73] LIM H Y, JEONG D, PARK S H, et al. Antiwrinkle and Antimelanogenesis Effects of Tyndallized *Lactobacillus* acidophilus KCCM12625P [J]. Int J Mol Sci, 2020, 21(5).

[74] KIM H M, LEE D E, PARK S D, et al. Oral administration of *Lactobacillus plantarum* HY7714 protects hairless mouse against ultraviolet B-induced photoaging [J]. J Microbiol Biotechnol, 2014, 24(11): 1583-91.

[75] KANO M, MASUOKA N, KAGA C, et al. Consecutive Intake of Fermented Milk Containing Bifidobacterium breve Strain Yakult and Galacto-oligosaccharides Benefits Skin Condition in Healthy Adult Women [J]. Biosci Microbiota Food Health, 2013, 32(1): 33-9.

[76] KANG Y M, HONG C H, KANG S H, et al. Anti-Photoaging Effect of Plant Extract Fermented with *Lactobacillus* buchneri on CCD-986sk Fibroblasts and HaCaT Keratinocytes [J]. J Funct Biomater, 2020, 11(1).

[77] FLAMAND N, MARROT L, BELAIDI J-P, et al. Development of genotoxicity test procedures with EpiSkin™®, a reconstructed human skin model: Towards new tools for in vitro risk assessment of dermally applied compounds? [J]. Mutation Research/Genetic Toxicology and Environmental Mutagenesis, 2006, 606(1): 39-51.

[78] JIN Y, CHENG X, HUANG X, et al. The role of Hrd1 in ultraviolet (UV) radiation induced photoaging [J]. Aging (Albany NY), 2020, 12(21): 21273-89.

[79] DANILENKO D M, PHILLIPS G D, DIAZ D. In Vitro Skin Models and Their Predictability in Defining Normal and Disease Biology, Pharmacology, and Toxicity [J]. Toxicol Pathol, 2016, 44(4): 555-63.

[80] BATAILLON M, LELIèVRE D, CHAPUIS A, et al. Characterization of a New Reconstructed Full Thickness Skin Model, T-Skin™, and its Application for Investigations of Anti-Aging Compounds [J]. Int J Mol Sci, 2019, 20(9).

[81] SANCHES V L, CUNHA T A, VIGANó J, et al. Comprehensive analysis of phenolics compounds in citrus fruits peels by UPLC-PDA and UPLC-Q/TOF MS using a fused-core column [J]. Food Chemistry: X, 2022, 14: 100262.

[82] PENG L Q, CAO J. Modern microextraction techniques for natural products [J]. Electrophoresis, 2021, 42(3): 219-32.

[83] JIANG M, DENG K, JIANG C, et al. Evaluation of the Antioxidative, Antibacterial, and Anti-Inflammatory Effects of the Aloe Fermentation Supernatant Containing *Lactobacillus plantarum* HM218749.1 [J]. Mediators Inflamm, 2016, 2016: 2945650.

[84] FILANNINO P, DI CAGNO R, TRANI A, et al. Lactic acid fermentation enriches the profile of biogenic compounds and enhances the functional features of common purslane (Portulaca oleracea L.) [J]. Journal of Functional Foods, 2017, 39: 175-85.

[85] ZHANG Y, ZHANG L, LIU J, et al. *Dendrobium officinale* leaves as a new antioxidant source [J]. Journal of Functional Foods, 2017, 37: 400-15.

[86] KIM D-H, CHOI H K, CHO S-C, et al. Enhancement of Antioxidant and Anti-aging Activities of Spirulina Extracts by Fermentation [J]. Journal of the Society of Cosmetic Scientists of Korea, 2008, 34.

[87] BERNERD F, ASSELINEAU D. An organotypic model of skin to study photodamage and photoprotection in vitro [J]. Journal of the American Academy of Dermatology, 2008, 58(5, Supplement 2): S155-S9.

[88] MARTIN R, PIERRARD C, LEJEUNE F, et al. Photoprotective effect of a water-soluble extract of Rosmarinus officinalis L. against UV-induced matrix metalloproteinase-1 in human dermal fibroblasts and reconstructed skin [J]. Eur J Dermatol, 2008, 18(2): 128-35.

Appendix

Table S Screening results of differential metabolites

Metab ID	Metabolite	VIP	FC(FDO /Control)	P-value	Regulate
metab_6613	16-Ketoestradiol	2.88	20.89	3.76E-06	up
metab_15650	Lucidenic acid K	2.47	2.55	0.002549	up
metab_6005	TOLFENAMIC ACID	3.35	2.38	0.003038	up
metab_3457	ANISODAMINE	3.10	2.04	0.002035	up
metab_11108	5-L-Glutamyl-L-alanine	3.50	2.01	4.69E-05	up
metab_6851	Madlongiside C	3.49	1.96	0.0001774	up
metab_7473	Norketamine	3.30	1.86	0.004225	up
metab_6801	Caproic acid	3.19	1.71	1.44E-06	up
metab_8859	Glycyl-Lysine	3.03	1.62	1.15E-06	up
metab_18852	Allithiamine	3.18	1.55	0.000192	up
metab_6922	(S)-Oleuropeic acid	2.03	1.52	0.02293	up
metab_8418	L-N2-(2-Carboxyethyl) arginine	2.73	1.51	6.16E-07	up
metab_3551	Agavoside A	2.83	1.50	1.82E-05	up
metab_7815	Bk-DMBDB	2.84	1.48	2.25E-06	up
metab_3305	Cytidine	2.67	1.48	0.00225	up
metab_7820	Deoxycytidine	1.89	1.47	0.0001047	up
metab_11450	Maltitol	2.84	1.47	0.003419	up
metab_11502	Fluticasone 17beta-carboxylic acid	2.97	1.45	7.59E-05	up
metab_480	Methyl cellulose	2.57	1.43	4.67E-05	up
metab_464	2,2,6,6-Tetramethyl-4-piperidinone	2.71	1.42	3.19E-06	up
metab_2740	Creatine	2.46	1.41	0.000618	up
metab_16829	(1S,2S,4R,8R)-p-Menthane-	2.57	1.41	6.75E-05	up

	1,2,8,9-tetrol				
metab_19392	Glucosamine	2.69	1.38	3.61E-06	up
metab_16966	3-Methyl-3-butenyl apiosyl-(1->6)-glucoside	2.02	1.37	0.04618	up
metab_8928	Cytosine	2.52	1.34	5.14E-05	up
metab_16323	(1S,3R,4R)-p-Menthane-1,3-diol	2.35	1.34	4.57E-05	up
metab_9470	Sterebin E	2.07	1.33	0.01632	up
metab_16007	Pubescenol	1.31	1.33	0.04567	up
metab_5832	10-hydroxy-2E-decenoic acid	1.82	1.33	0.0208	up
metab_2855	Hypoxanthine	2.29	1.32	6.81E-06	up
metab_8692	N2-(D-1-Carboxyethyl)-L-lysine	2.20	1.32	0.0001614	up
metab_3330	Isoleucyl-Hydroxyproline	2.24	1.31	0.00167	up
metab_11571	Uric acid	2.04	1.31	0.03976	up
metab_18071	4-hydroxy-3-(sulfooxy)benzoic acid	2.09	1.28	0.002035	up
metab_11428	Hydantoin-5-propionic acid	2.23	1.27	3.40E-05	up
metab_11507	1-(Malonylamino)cyclopropanecarboxylic acid	2.51	1.26	7.67E-06	up
metab_13426	4-hydroxy ketorolac	2.20	1.26	0.00941	up
metab_469	Alanyl-Threonine	2.12	1.25	4.09E-05	up
metab_5980	Cyclic 6-Hydroxymelatonin	1.88	1.24	7.25E-07	up
metab_9993	3,4-Dimethyl-5-pentyl-2-furanpropanoic acid	2.25	1.23	0.0004833	up
metab_18884	Gamma-Carboxyglutamic acid	1.67	1.23	0.008334	up
metab_194	Ophiopogonin C'	2.10	1.23	0.0001542	up
metab_206	Demethylsulochrin	1.51	1.22	0.02965	up
metab_3017	Succinylmonocholine	2.01	1.22	2.02E-05	up
metab_15795	N-desisopropylpropranolol	1.42	1.21	0.03835	up

metab_6713	2-hydroxy-3-phenylpropanal	1.83	1.21	0.01095	up
metab_11997	(2S,2'S)-Pyrosaccharopine	2.01	1.21	0.004003	up
metab_18636	Glutamylglutamine	2.09	1.21	1.40E-07	up
metab_18453	8-[(Aminomethyl)sulfanyl]-6-sulfanyloctanoic acid	2.37	1.21	1.01E-07	up
metab_1294	Prolyl-Glutamine	1.65	1.20	0.001247	up
metab_17936	Glycylprolylhydroxyproline	2.04	1.20	0.0002364	up
metab_1371	[6]-Dehydrogingerdione	1.68	1.19	0.001776	up
metab_11029	N-gamma-Glutamylglutamine	1.87	1.19	0.003062	up
metab_395	(E)-2-Butenyl-4-methyl-threonine	1.97	1.19	6.41E-06	up
metab_8326	Prolyl-Histidine	1.87	1.19	8.65E-05	up
metab_6274	Hydroxyltolmetin	1.57	1.17	0.002964	up
metab_12230	Caffeoyl C1-glucuronide	1.68	1.17	0.005487	up
metab_12080	L-alpha-Hydroxyisovaleric acid	1.69	1.16	0.00189	up
metab_15970	(4R,5S,7R,11x)-11,12-Dihydroxy-1(10)-spirovetiven-2-one 12-glucoside	1.73	1.15	0.006269	up
metab_19173	2,6-diaminohexanoic acid	1.75	1.15	0.0004248	up
metab_11358	L-2-Amino-5-hydroxypentanoic acid	1.70	1.15	1.06E-05	up
metab_7375	3-Aminoquinoline	1.31	1.15	0.02134	up
metab_11618	Glutamylglycine	1.80	1.14	7.71E-05	up
metab_8233	Lentiginosine	1.65	1.14	0.0005259	up
metab_9662	L-Galacto-2-heptulose	2.03	1.14	3.60E-06	up
metab_1537	Phenylalanylproline	1.69	1.14	6.79E-05	up
metab_13997	Cis-9,10-Epoxystearic acid	1.63	1.14	0.04083	up
metab_8944	L-Carnitine	1.67	1.13	0.001642	up
metab_18862	Aspartyl-Asparagine	1.64	1.13	0.002397	up

metab_17817	L-beta-aspartyl-L-leucine	1.70	1.13	0.0006919	up
metab_18460	Gamma-Glutamylalanine	1.73	1.12	1.37E-05	up
metab_9697	Ribothymidine	1.77	1.12	0.0001399	up
metab_11590	5-Methyldeoxycytidine	1.53	1.12	0.007206	up
metab_91	Adenine	1.63	1.12	7.27E-05	up
metab_2730	2-(1-Aziridinyl)ethanol	1.39	1.11	0.0001771	up
metab_7791	7-hydroxy-2-(3-hydroxyphenyl)-4H-chromen-4-one	1.28	1.11	0.0003906	up
metab_11965	Gamma-Glutamylvaline	1.75	1.11	0.0002416	up
metab_19169	L-Arginine	1.67	1.11	6.37E-05	up
metab_18958	Galactosylglycerol	1.65	1.11	1.66E-06	up
metab_17107	(3R,5Z)-5-Octene-1,3-diol	1.33	1.11	0.01323	up
metab_9427	(2S,3'S)-alpha-Amino-2-carboxy-5-oxo-1-pyrrolidinebutanoic acid	1.61	1.11	0.0003785	up
metab_17385	5-Methoxytryptamine	1.41	1.11	0.00358	up
metab_17584	3-Phenylpropionylglycine	1.45	1.11	0.001465	up
metab_402	Phenylacetaldehyde	1.63	1.10	1.59E-06	up
metab_7682	Guanine	1.01	1.10	0.02376	up
metab_6247	Amprotropine	1.17	1.10	0.04761	up
metab_5584	Dihydroceramide	1.09	1.10	0.02525	up
metab_10898	Glutamylproline	1.53	1.10	0.0002145	up
metab_17632	Gamma-Glu-Leu	1.44	1.10	0.008569	up
metab_18694	L-4-Hydroxyglutamate semialdehyde	1.75	1.10	5.37E-05	up
metab_9323	L-Glutamate	1.40	1.10	2.16E-05	up
metab_19381	1-Pyrroline-5-carboxylic acid	1.34	1.10	0.01481	up
metab_8636	T-4-AMINOCROTONIC ACID (TACA)	1.31	1.10	0.002021	up

metab_8328	L-prolyl-L-proline	1.38	1.10	0.0002203	up
metab_5669	Avocadene	1.22	1.09	0.0369	up
metab_12468	Tanacetol A	1.31	1.09	0.01242	up
metab_437	2-Hexen-1-ol	1.23	1.09	0.01795	up
metab_18708	3-Hydroxypicolinic acid	1.41	1.09	0.0003578	up
metab_10697	Atrolactic acid	1.46	1.09	0.0005554	up
metab_17893	S-Lactoylglutathione	1.46	1.09	0.001792	up
metab_8519	(S)-2-Azetidinecarboxylic acid	1.34	1.08	0.001722	up
metab_7042	L-Pyridosine	1.25	1.08	0.0005153	up
metab_10976	N-Acetyl-L-glutamic acid	1.40	1.08	0.0003612	up
metab_18831	3-methyl-4-(sulfooxy)but-2-enoic acid	1.17	1.08	0.002041	up
metab_3129	Melledonol	1.26	1.08	0.0001058	up
metab_2412	Austdiol	1.21	1.08	0.000508	up
metab_17504	5-(2-Methylpropyl)tetrahydro-2-oxo-3-furancarboxylic acid	1.23	1.08	0.007652	up
metab_3005	N-Acetyl-b-glucosaminylamine	1.21	1.08	0.001167	up
metab_18724	Guanidylic acid (guanosine monophosphate)	1.33	1.08	0.002898	up
metab_2118	Isoleucylproline	1.34	1.08	0.0009937	up
metab_8516	(R)-(+)-2-Pyrrolidone-5-carboxylic acid	1.33	1.08	0.001391	up
metab_17332	Tetrahydroneopterin	1.15	1.07	0.03005	up
metab_8884	ACEXAMIC ACID	1.03	1.07	0.02706	up
metab_12097	N-lactoyl-Valine	1.06	1.07	0.02989	up
metab_11081	5'-CMP	1.32	1.07	0.000337	up
metab_19053	Ribitol	1.23	1.07	6.10E-05	up
metab_8252	AMINOHYDROXYBUTYRIC ACID	1.08	1.07	0.004939	up

metab_7194	2-amino-m-cresol	1.04	1.07	0.0002142	up
metab_9382	Tetrahydrodipicolinate	1.23	1.07	0.002431	up
metab_7919	Phe Ala	1.14	1.07	0.00306	up
metab_1312	2-Naphthylamine	1.12	1.07	0.02237	up
metab_9372	Maltotetraose	1.42	1.07	1.97E-05	up
metab_735	Gamma-Glutamylglycine	1.18	1.07	0.001713	up
metab_8983	Beta-Alanine	1.13	1.07	0.0001768	up
metab_8091	1-(2-Furyl)butan-3-one	1.15	1.07	0.003301	up
metab_11834	2-oxo-3-(2,4,5-trihydroxyphenyl)propanoic acid	1.11	1.06	0.04219	up
metab_8657	Dimethylethanolamine	1.14	1.06	0.002215	up
metab_11146	Daucic acid	1.34	1.06	7.81E-05	up
metab_18704	Acetylhomoserine	1.11	1.06	0.006897	up
metab_5408	N,N-(2,2-dihydroxy-ethyl) arachidonoyl amine	1.03	1.06	0.03871	up
metab_8232	SALSOLINE	1.08	1.06	0.0005321	up
metab_8730	N-butanoyl-lhomoserine lactone	1.09	1.06	0.008788	up
metab_18250	Normetanephrine	1.26	1.06	0.004698	up
metab_10895	Indoleacrylic acid	1.00	1.06	0.04748	up
metab_11964	L-Dopa	1.08	1.06	0.02209	up
metab_8881	Valyl-Hydroxyproline	1.03	1.06	0.001399	up
metab_7986	N-ACETYLPROLINE	1.06	1.06	0.0003027	up
metab_19390	Dulcitol	1.21	1.05	2.64E-05	up
metab_11736	Gamma-Glutamylproline	1.01	1.05	0.01043	up
metab_9420	Molybdopterin precursor Z	1.13	1.05	0.01348	up
metab_17815	3,4,5-trihydroxy-6-[(2-methylpropanoyl)oxy]oxane-2-carboxylic acid	1.01	1.05	0.01409	up
metab_11471	KOJIC ACID	1.05	1.05	0.001206	up

metab_9678	Adenosine 3'-monophosphate	1.08	1.05	0.0003635	up
metab_19387	D-Tartaric acid	1.16	1.05	0.00467	up
metab_9716	N-lactoyl-Leucine	1.07	1.04	0.008995	up
metab_17572	Diosbulbinoside F	1.02	1.04	0.001504	up
metab_9380	Shikimic acid	1.06	1.04	0.007211	up
metab_18844	Erythrono-1,4-lactone	1.01	1.04	0.003403	up
metab_19394	Isocitrate	1.22	0.96	0.001115	down
metab_19049	Gluconic acid	1.28	0.95	0.0007122	down
metab_136	3,4,5-trihydroxy-6-(2-oxoethoxy)oxane-2-carboxylic acid	1.12	0.95	4.76E-05	down
metab_9039	6-Succinoaminopurine	1.04	0.95	7.35E-05	down
metab_2457	6-(butanoyloxy)-3,4,5-trihydroxyoxane-2-carboxylic acid	1.09	0.95	0.0005003	down
metab_11367	Arabinofuranobiose	1.26	0.94	0.0003885	down
metab_11354	7,8-Dihydroneopterin	1.24	0.94	0.0009492	down
metab_2701	5-Ethyl-2,3-dimethylpyrazine	1.06	0.94	0.0004543	down
metab_9012	Lysinoalanine	1.10	0.94	0.0004484	down
metab_11075	3-Keto-b-D-galactose	1.49	0.93	0.001032	down
metab_7836	2-Phthalimidoglutaric acid	1.06	0.93	9.76E-06	down
metab_2474	Thymine	1.21	0.93	0.0003834	down
metab_19035	2-methyl-3-(sulfooxy)propanoic acid	1.29	0.93	0.0001547	down
metab_11603	Xanthine	1.11	0.93	0.03157	down
metab_8573	2,5-Furandicarboxylic acid	1.26	0.93	0.003009	down
metab_174	D-Glucaro-1,4-lactone	1.33	0.92	6.08E-05	down
metab_8361	2-Pyrrolidineacetic acid	1.15	0.92	0.03105	down
metab_14936	PE(18:2/0:0)	1.47	0.91	0.003429	down

metab_5608	18R-HEPE	1.28	0.91	0.03999	down
metab_11556	Oxaloacetate	1.44	0.91	0.007002	down
metab_9685	Uridine	1.79	0.90	0.001469	down
metab_2043	PC(18:2/0:0)	1.55	0.89	0.03116	down
metab_10509	LysoPC(18:2(9Z,12Z))	1.67	0.88	0.04216	down
metab_5521	MG(0:0/18:3(6Z,9Z,12Z)/0:0)	1.59	0.88	0.003933	down
metab_19032	D-Glucarate	1.70	0.88	0.0003829	down
metab_1167	Ile Pro Tyr	1.78	0.86	7.82E-05	down
metab_6142	(6E,8E)-4,6,8-Megastigmatriene	1.06	0.85	0.03963	down
metab_17928	Ala Gly Leu Val Ser	1.90	0.84	0.00609	down
metab_1623	Ile Val Ile	1.79	0.84	0.0152	down
metab_19396	Malic acid	2.44	0.84	0.000286	down
metab_8287	4-Hydroxybenzaldehyde	1.85	0.84	0.00303	down
metab_1587	Tyr Leu Val Phe	1.81	0.83	0.03675	down
metab_9019	L-Asparagine	1.84	0.83	5.03E-05	down
metab_1462	Beta-Carotinal	1.74	0.83	0.03566	down
metab_8077	2-Amino-3-carboxymuconic acid semialdehyde	1.35	0.83	0.03988	down
metab_9317	2-Hydroxycinnamic acid	1.99	0.82	0.008006	down
metab_1261	Ile Trp Ala Ser	1.91	0.80	0.01519	down
metab_1472	Ala Leu Ala Trp	2.18	0.78	0.005346	down
metab_3160	Dynorphin A (6-8)	2.17	0.75	0.02824	down
metab_403	Guanosine	2.34	0.74	0.01091	down
metab_2418	Asn Tyr Leu Asn	2.48	0.71	0.000392	down
metab_18748	3,4,5-trihydroxy-6-[(2-hydroxyacetyl)oxy]oxane-2-carboxylic acid	2.77	0.70	0.0002396	down
metab_11985	Suberylglycine	2.95	0.67	1.32E-05	down
metab_223	3,5,7-trihydroxy-2-(3-hydroxy-5-	1.72	0.66	0.01033	down

	methoxyphenyl)-3,4-dihydro-2H-1-benzopyran-4-one				
metab_15268	11-dehydro-TXB3	2.53	0.50	0.004216	down
metab_15233	Cofaryloside	2.65	0.46	0.0009433	down

Dissertation based on the original work

Fei W, Noda M, Danshiitsoodol N, and Sugiyama, M. *Dendrobium officinale* extract fermented with *Lactobacillus plantarum* GT-17F enhances the protection of UV-mediated photoaging. Biol Pharm Bull, 46, 1451–1460 (2023).

Acknowledgements

When I was about to start my Ph.D., the COVID-19 epidemic happened. During this time, I was confused and didn't know what to do. Fortunately, with everyone's help, I still completed my whole graduate study! I want to express my deepest gratitude to everyone who has supported and guided me.

For this study, I would like to thank the Hiroshima University, Graduate School for Biomedical and Health Sciences, Department of Probiotic Sciences for Preventive Medicine, Prof. Masanori Sugiyama. He lets me into the research field of *Lactobacillus plantarum* and has always given me sincere guidance and encouragement. His profound knowledge, inspiring inculcation and persistent strict requirements stimulated my enthusiasm for my research topic and thesis. Without her enlightened guidance and patient revision, my thesis would not have been possible.

I would also like to thank the Department of Probiotic Sciences for Preventive Medicine Associate Professors Masafumi Noda and Narandalai Danshiitsoodol, who gave me a lot of inspiration and suggestions during my research and graduation preparation.

In addition to the mentors, I would also like to thank my wonderful laboratory partners whose support has always been my motivation. Whether conducted through a screen during lockdown or under laboratory conditions, it provided a lifeline at the most difficult times. I am proud to say that we are not just lab mates, but good friends.

Finally, I would also like to thank my family. With their support, I successfully completed the whole graduate study.